JOURNAL OF PETROLOGY | VOLUME 48 | NUMBER 10 | PAGES 1843–1873 | 2007 | doi:10.1093/petrology/egm041

Origins of Xenolithic Eclogites and Pyroxenites from the Central Slave Craton, Canada

SONJA AULBACH[1]*, NORMAN J. PEARSON[1], SUZANNE Y. O'REILLY[1] AND BUDDY J. DOYLE[2]

[1]GEMOC ARC NATIONAL KEY CENTRE, DEPARTMENT OF EARTH AND PLANETARY SCIENCES, MACQUARIE UNIVERSITY, NSW 2109, AUSTRALIA

[2]LITHOSPHERE SERVICES, 4009 EDINBURGH STREET, BURNABY, BC, CANADA V5C 1R4

RECEIVED SEPTEMBER 27, 2006; ACCEPTED JULY 4, 2007
ADVANCE ACCESS PUBLICATION SEPTEMBER 3, 2007

Major- and trace-element and Sr–Nd–Hf isotopic compositions of garnet and clinopyroxene in kimberlite-borne eclogite and pyroxenite xenoliths were used to establish their origins and evolution in the subcontinental lithospheric mantle beneath the central Slave Craton, Canada. The majority of eclogites can be assigned to three groups (high-Mg, high-Ca or low-Mg eclogites) that have distinct trace-element patterns. Although post-formation metasomatism involving high field strength element (HFSE) and light rare earth element (LREE) addition has partially obscured the primary compositional features of the high-Mg and high-Ca eclogites, trace-element features, such as unfractionated middle REE (MREE) to heavy REE (HREE) patterns suggestive of garnet-free residues and low Zr/Sm consistent with plagioclase accumulation, could indicate a subduction origin from a broadly gabbroic protolith. In this scenario, the low ∑REE and small positive Eu anomalies of the high-Mg eclogites suggest more primitive, plagioclase-rich protoliths, whereas the high-Ca eclogites are proposed to have more evolved protoliths with higher (normative) clinopyroxene/plagioclase ratios plus trapped melt, consistent with their lower Mg-numbers, higher ∑REE and absence of Eu anomalies. In contrast, the subchondritic Zr/Hf and positive slope in the HREE of the low-Mg eclogites are similar to Archaean second-stage melts and point to a previously depleted source for their precursors. Low ratios of fluid-mobile to less fluid-mobile elements and of LREE to HREE are consistent with dehydration and partial melt loss for some eclogites. The trace-element characteristics of the different eclogite types translate into lower ε_{Nd} for high-Mg eclogites than for low-Mg eclogites. Within the low-Mg group, samples that show evidence for metasomatic enrichment in LREE and HFSE have lower ε_{Nd} and ε_{Hf} than a sample that was apparently not enriched, pointing to long-term evolution at their respective parent–daughter ratios. Garnet and clinopyroxene in pyroxenites show different major-element relationships from those in eclogites, such as an opposite CaO–Na_2O trend and the presence of a CaO–Cr_2O_3 trend, independent of whether or not opx is part of the assemblage. Therefore, these two rock types are probably not related by fractionation processes. The presence of opx in about half of the samples precludes direct crystallization from eclogite-derived melts. They probably formed from hybridized melts that reacted with the peridotitic mantle.

KEY WORDS: *eclogites; pyroxenite xenoliths; mantle xenoliths; eclogite trace elements; eclogite Sr isotopes; eclogite Hf isotopes; eclogite Nd isotopes*

INTRODUCTION

Eclogites are a volumetrically small but compositionally significant component in the mantle because of their fertile composition, rapidly evolving radiogenic isotope compositions (as a result of parent–daughter ratios distinct from depleted or primitive upper mantle reservoirs), and lower melting point relative to peridotite, making them a source of isotopically distinct components in the refractory continental lithosphere. In addition, the presence of eclogites in the mantle column indicates the operation of processes that are likely to have significantly affected the lithosphere, regardless of their origin.

There are two main hypotheses for the origin of kimberlite-borne eclogite xenoliths [for a recent review, see Jacob (2004)]: they might have an intrusive high-pressure mantle melt origin (e.g. Hills & Haggerty, 1989; Smyth *et al.*, 1989; Caporuscio & Smyth, 1990;

*Corresponding author. Present address: Earth and Atmospheric Sciences, University of Alberta, Edmonton, AB, T6G 2E3, Canada. Telephone: +61 2 9850 8953. Fax: +61 2 9850 8943. E-mail: saulbach@els.mq.edu.au

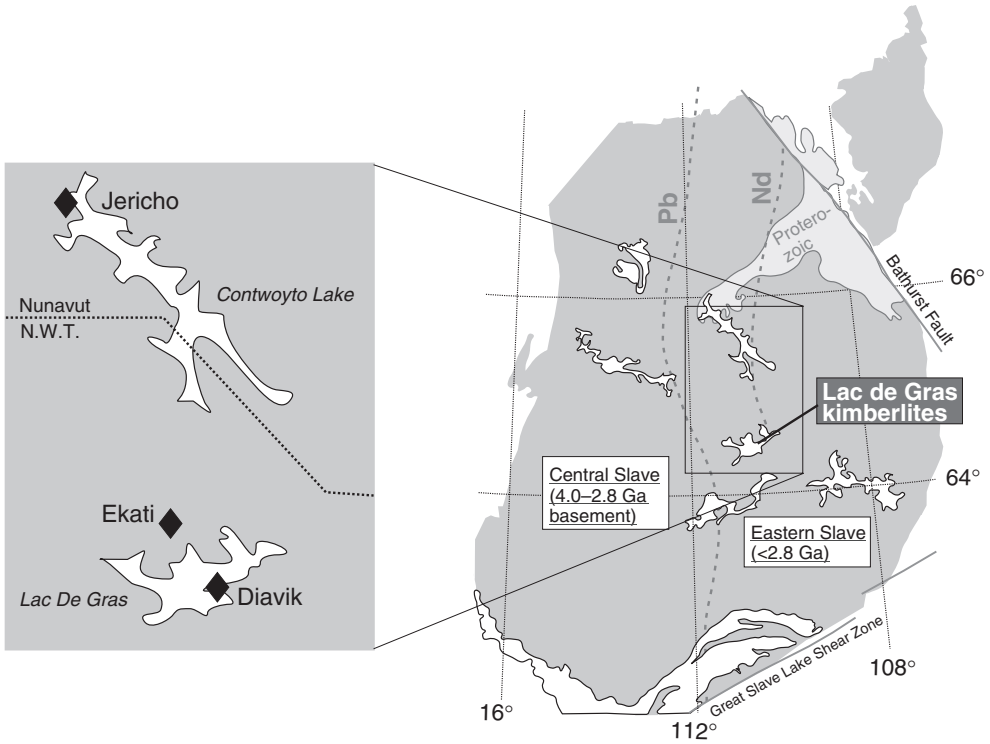

Fig. 1. Map of the Slave Craton (after Davis *et al.*, 2003) showing Pb and Nd isotope lines that separate ancient basement in the west from juvenile rocks in the east. Localities of the Diavik, Ekati and Jericho kimberlites are shown in more detail on the left.

Griffin & O'Reilly, 2007), or represent subducted oceanic crust (e.g. MacGregor & Manton, 1986; Schulze & Helmstaedt, 1988; Jacob *et al.*, 1994; Beard *et al.*, 1996). Eclogite suites from many localities in the Kaapvaal and Siberian cratons fall into groups, with one group having characteristics consistent with a mantle origin whereas another group (or groups) has been interpreted as crustally derived (Taylor & Neal, 1989; Viljoen *et al.*, 1996; Kopylova *et al.*, 1999; Barth *et al.*, 2002*b*). In addition to primary differences, eclogite compositions can be modified during melting and metasomatism following their formation (Ireland *et al.*, 1994; Barth *et al.*, 2001).

We have carried out a detailed petrographic, major- and trace-element and multi-isotope study to constrain the genesis of different eclogite xenolith types found in kimberlites intruded in the central Slave Craton, Canada, bearing in mind that they may have been subjected to a range of post-formation processes during their residence time in the Archaean lithosphere, including melting and metasomatic overprinting.

GEOLOGICAL SETTING

The samples are derived from the Diavik A154 kimberlite pipe, in the Lac de Gras area of the Slave Craton in the Canadian Northwest Territories (Fig. 1). The Slave Craton is a small (400 km × 500 km) Archean block that is composed of two major basement domains: (1) a Hadean to Mesoarcheaean domain in the west (Central Slave Basement Complex, CSBC; Bleeker *et al.*, 1999) with ages of 4·0–2·8 Ga, onto which 2·73–2·70 Ga tholeiites were extruded (Padgham & Fyson, 1992; van Breemen *et al.*, 1992; Isachsen & Bowring, 1994); (2) a Neoarchaean, isotopically juvenile domain in the east, where the tholeiite sequence is notably absent. The Mesoarchaean basement, the eastern extent of which is not accurately known, dips under the eastern domain (Bleeker *et al.*, 1999). The origin of these domains has been ascribed to arc–continent collision (Kusky, 1989; Davis & Hegner, 1992) or to the eastern domain representing attenuated, modified Mesoarchaean lithosphere (Bleeker, 2003). A major north–south-trending provinciality in the Slave Craton is evident in basement Nd and Pb isotope data (Davis & Hegner, 1992) and a coupling of the two domains by ~2·7 Ga may be indicated by pan-Slave calc-alkaline volcanism (van Breemen *et al.*, 1992). Younger events include 2·2–1·8 Ga collisions with neighbouring terranes (Hoffman, 1989), numerous episodes of Proterozoic dike emplacement, such as the Malley–McKay dike swarm at 2·21–2·23 Ga (LeCheminant *et al.*, 1996) and the 1·27 Ga Mackenzie swarm (LeCheminant & Heaman, 1989), followed by kimberlite volcanism in Cretaceous to Eocene time (Creaser *et al.*, 2004; Heaman *et al.*, 2004).

Distinct mantle xenolith suites and spatial distributions of mantle rock types in the lithosphere beneath different

parts of the craton have been recognized (Griffin *et al.*, 1999, 2004; Grütter *et al.*, 1999; Kopylova *et al.*, 1999; MacKenzie & Canil, 1999; Pearson *et al.*, 1999; Carbno & Canil, 2002), which have been substantiated by magnetotelluric and elastic thickness data (Jones *et al.*, 2001; Poudjom Djomani *et al.*, 2005). Here, we focus on our current knowledge of the mantle evolution in the central Slave Craton, 340 km NE from Yellowknife, NT, where the Lac de Gras kimberlites were intruded. The subcontinental lithospheric mantle (SCLM) sampled by the Lac de Gras kimberlites is strongly layered, with an ultra-depleted shallow layer and a less depleted deep layer, the latter suggested to have formed by subcretion of a plume head that delivered diamonds containing lower mantle inclusions (Griffin *et al.*, 1999, 2004; Davies *et al.*, 1999; Aulbach *et al.*, 2007). A Re–Os isochron age of 3·27 ± 0·34 Ga for some sulfides from the deep layer may date the formation of this layer and shows that significantly older mantle resides beneath some of the 2·7 Ga crust of the juvenile eastern domain (Contwoyto Terrane) in the Slave Craton (Aulbach *et al.*, 2004*a*). This isochron age agrees, within uncertainty, with one derived from sulfide inclusions in diamonds from the Panda kimberlite (Westerlund *et al.*, 2006), just north of Lac de Gras, and is consistent with previous findings that many kimberlites lying in the younger, eastern domain appear to have sampled older lower crust and mantle, indicative of an east-dipping trans-lithospheric boundary dating back to 2·7 Ga craton amalgamation (Grütter *et al.*, 1999; Irvine *et al.*, 2003).

SAMPLES AND ANALYTICAL TECHNIQUES

All samples of the present study were retrieved from drill core of kimberlite pipe A154S in the Lac de Gras area, from depths between ~100 and 470 m. Samples of at least 1 cm in size were cut out of the drill core and processed, to minimize sampling bias, although this possibly discriminates against more friable eclogite types that are not as well preserved. Eighteen eclogites and pyroxenites were selected for the present study and results combined with those of Pearson *et al.* (1999, and unpublished data) to make up a total of 35 eclogites and 30 pyroxenites.

Major-element analyses were obtained using a CAMECA Camebax SX50 electron microprobe. *In situ* trace-element compositions were determined with a custom-built laser-ablation system (designed by S. E. Jackson) or a Merchantek LUV 266 Nd:YAG UV laser system, both linked to an Agilent 7500 inductively coupled plasma mass spectrometry (ICP-MS) system and reduced using the GLITTER software (van Achterberg *et al.*, 1999). Accuracy and precision were monitored by analysing basalt standard BCR-2G with each batch of samples as an unknown. Results, standard deviations and detection limits are given in Electronic Appendix 1, which can be downloaded from http://petrology.oxfordjournals.org/. Sr–Nd–Hf isotope data for garnet and clinopyroxene (cpx) separates, leached and ultrasonicated in 6N HCl for 30 min followed by ultrasonication in three aliquots of MQ, prior to dissolution were obtained using a Nu Plasma multi-collector (MC) ICP-MS system. All analytical work was carried out in the GEMOC National Key Centre at Macquarie University (www.es.mq.edu.au/GEMOC/) following the techniques described by Aulbach *et al.* (2004*b*). Repeated measurements of standard materials during data acquisition (February–July 2003) yielded the following values: $^{87}Sr/^{86}Sr$ of 0·710257 ± 0·000045 (2 SD; $n = 42$) for the SRM-987 standard; $^{87}Sr/^{86}Sr$ of 0·70352 ± 0·000040 ($n = 15$) for BHVO-1; $^{143}Nd/^{144}Nd$ of 0·511138 ± 0·000038 ($n = 42$) for the JMC-321 standard, $^{143}Nd/^{144}Nd$ of 0·513003 ± 0·000043 ($n = 10$) for BHVO-1; $^{176}Hf/^{177}Hf$ of 0·282163 ± 0·000002 ($n = 20$) for the JMC-475 standard and $^{176}Hf/^{177}Hf$ of 0·283128 ± 0·000090 for BHVO-1 ($n = 8$) (Aulbach *et al.*, 2004*b*).

Although the uncertainties of Sr and Nd isotope ratios for pure Sr and Nd standards obtained by MC-ICP-MS are two to three times higher than those reported for thermal ionization mass spectrometry (TIMS) measurements (http://georem.mpch-mainz.gwdg.de/), they are adequate for the samples analysed in the present study, which mostly have significantly evolved isotopic compositions compared with depleted mantle or CHUR. The significantly higher uncertainty for $^{176}Hf/^{177}Hf$ of the rock standard than for the pure Hf standard may reflect matrix interference as a result of imperfectly purified solutions (e.g. Blichert-Toft *et al.*, 1997).

PETROGRAPHY AND CLASSIFICATION

The petrography of the studied eclogites from Lac de Gras is summarized in Table 1. The majority of samples that were large enough to obtain microstructural information have medium- to coarse-grained granoblastic microstructures. Three eclogites have a weakly tabular microstructure, which is due to the weak elongation and subparallel alignment of garnet and cpx in sample YK3528 and to the preferred orientation of phlogopite in samples VR19674ecl-g7 and YK1911.

Most samples are fresh or show minor (<10%) alteration that is restricted to veins and grain boundaries. A few samples are more strongly altered, with pyroxenes usually more affected than garnet. Altered areas are composed of small secondary phlogopite, sulfide flakes and unidentifiable microcrystalline phases with a felty brown to green appearance.

Table 1: Petrographic data and eclogite classification

Sample no.	Ref.[1]	Type[2]	$Gp_{M\&G}$[3]	$Gp_{T\&N}$[4]	Size[5]	Microstructure[6]	Assemblage/mode[7]						
							gt	cpx	rut	sf	ky	opx	other
Eclogites													
SE01	3	high-Mg	I	A	<1	n.a.	x	x					
SE02	3	high-Ca	I	B	<1	n.a.	x	x		x			
SE03	3	high-Mg	II	A	<1	n.a.	x	x					
SE04	3	high-Mg	II	B	<1	n.a.	x	x					
SE11	3	low-Mg	II	B	<1	n.a.	x	x	x	x			
vr09399	2	high-Mg	II	A	<1	n.a.	x	x					
vr19674ecl-g4	2	low-Mg	II	B	1·6	n.a.	x	x					
vr19674ecl-g5	2*	high-Ca	II	C	<1	n.a.	x	x					
vr19674ecl-g6	2	high-Mg	I	A	<1	n.a.	x	x					
vr19674ecl-g7	1	volatile-rich	II	A	1·5	medium-tabular							phlog (44), ap (<1)
vr19677ecl-g1	2	high-Mg	II	B	<1	n.a.	x	x					
vr19677ecl-g2	2	high-Mg	II	B	1·7	n.a.	x	x	x				
vr19677ecl-g4	2	high-Mg	II	B	<1	n.a.	x	x					
vr19677ecl-g5	2	high-Mg	I	B	<1	n.a.	x	x					
vr19677ecl-g6	2	high-Mg	II	A	<1	n.a.	x	x					
vr40345	3	high-Ca	I	B	<1	n.a.	x	x			x		dia (trace)
vr40364	2	high-Mg	II	A	<1	n.a.	x	x					
vr43452	1	low-Mg	I	B	4·5	coarse-grano	48	51	1				
vr43465	1	high-Ca	I	B	2	coarse-grano	41	55		1			graph (3)
vr43469	1	low-Mg	II	B	1·5	coarse-grano	60	40	<1	<1			
vr43477	1	low-Mg	II	B	1·5	coarse-grano	x	x		x			
vr43479	1	low-Mg	II	A	2·5	medium-grano	50	50		<1			
vr43480	1	high-Mg	I	A	2	medium-grano	89	11	<1				
vr50858	2*	high-Ca	II	B	<1	n.a.	x	x			x		
vr50860	2*	high-Ca	I	C	<1	n.a.	x	x					
vr50909	3	high-Ca	II	B	<1	n.a.	x	x	x		x		
vr50916	2	high-Mg	II	A	<1	n.a.	x	x					
vr67112b	1	volatile-rich	II	C	2	medium-grano				<1			ilm (3), cc (2)
vr67360	1	high-Mg	II	A	3	coarse-grano	62	38		<1			
yk1911	1	volatile-rich	II	B	2	medium-tabular	31	18					phlog (49), ap (<1), plag (<1), cc (<1)
yk1926	1	low-Mg	II	B	1·7	coarse-grano	70	30	<1				
yk1943	1	low-Mg	I	B	2	coarse-grano	57	41	2	<1			qz (<1)
yk1946	1	high-Mg	II	A	3	coarse-grano	62	37	1	<1			
yk1949	1	high-Mg	II	B	3	coarse-grano	70	30	<1	<1			
yk3528	1	high-Ca	I	B	2·5	medium-tabular	57	43	<1				
Pyroxenites													
SE08	3	n.a.	II	A	<1	n.a.	x	x					
SE09	3	n.a.	II	A	<1	n.a.	x	x		x			
vr09353	2	n.a.	II	A	<1	n.a.	x	x				x	
vr09384	2*	n.a.	II	B	<1	n.a.	x	x				x	
vr09405	2	n.a.	II	A	<1	n.a.	x	x					
vr09406	2	n.a.	II	A	<1	n.a.	x	x				x	
vr09424	3	n.a.	II	A	<1	n.a.	x	x				x	

(continued)

Table 1: Continued

Sample no.	Ref.[1]	Type[2]	$Gp_{M\&G}$[3]	$Gp_{T\&N}$[4]	Size[5]	Microstructure[6]	Assemblage/mode[7]						
							gt	cpx	rut	sf	ky	opx	other
vr19673ecl-g1	2*	n.a.	II	B	<1	n.a.	x	x				x	
vr19673ecl-g2	2	n.a.	II	B	<1	n.a.	x	x	x			x	
vr19674ecl-g1	2	n.a.	II	A	<1	n.a.	x	x				x	
vr19674ecl-g2	2	n.a.	II	A	<1	n.a.	x	x				x	
vr19674ecl-g3	2	n.a.	II	A	<1	n.a.	x	x					
vr19674per-g1	2	n.a.	II	A	<1	n.a.	x	x					
vr19674per-g4	2	n.a.	II	A	<1	n.a.	x	x				x	
vr40302	2	n.a.	II	A	<1	n.a.	x	x				x	
vr40336	3	n.a.	II	A	<1	n.a.	x	x				x	
vr40337	2	n.a.	I	A	<1	n.a.	x	x					
vr40374	2	n.a.	II	A	<1	n.a.	x	x				x	
vr40382	2	n.a.	II	A	<1	n.a.	x	x				x	
vr40384 ecl-g4	2	n.a.	II	A	<1	n.a.	x	x	x				
vr40399	2	n.a.	II	B	<1	n.a.	x	x	x				
vr50856	2	n.a.	II	A	<1	n.a.	x	x				x	
vr50887	2	n.a.	II	A	<1	n.a.	x	x					
vr50888	2	n.a.	II	A	<1	n.a.	x	x					
vr50899	2	n.a.	II	A	<1	n.a.	x	x				x	
vr50900	2	n.a.	II	A	<1	n.a.	x	x				x	
vr50925	2	n.a.	II	B	<1	n.a.	x	x					
yk1914	1	n.a.	II	A	2·5	medium-grano	22	78					
yk1915	1	n.a.	II	A	1·5	coarse-grano	x		x	x		x	
yk1952	1	n.a.	II	A	2	medium-grano	x	x		x		x	

[1]References: 1, this study; 2, Pearson *et al*. (1999); 3, Pearson *et al*. (unpublished data); *trace-element analyses this study.
[2]Classification based on chemical parameters (see text for details).
[3]Classification of McCandless & Gurney (1989), based on MacGregor & Carter (1970).
[4]Classification of Taylor & Neal (1989), based on Coleman *et al*. (1965).
[5]Longest dimension (cm) across xenolith.
[6]Only given for samples >1 cm in size; grano, granoblastic.
[7]Modes (vol. %) are given where available, otherwise presence of mineral is indicated as identified in thin section or stub; gt, garnet; cpx, clinopyroxene; ky, kyanite; rut, rutile; sulf, sulfide; phlog, phlogopite; ap, apatite; dia, diamond; graph, graphite; cc, calcite; ilm, ilmenite; pl, plagioclase; qz, quartz; opx, orthopyroxene; n.a., not applicable or not available.

Some xenoliths have subhedral or rounded garnets in a 'matrix' of interstitial cpx (Group I of MacGregor & Carter, 1970; Fig. 2a), whereas in others garnet and cpx have straight grain boundaries and an interlocking fabric (Group II; Fig. 2b). The classification of McCandless & Gurney (1989) builds on work of MacGregor & Carter (1970) and distinguishes group I eclogites by their higher Na_2O in garnet (≥0·09 wt %) and K_2O in cpx (≥0·08 wt %) from group II eclogites. The classification used in Table 1 ($Gp_{M\&G}$) is that based on Na_2O contents in garnet. A different classification ($Gp_{T\&N}$) places eclogites into groups A, B and C, distinguished by the MgO, FeO and CaO contents of garnets and Na_2O and MgO contents of clinopyroxenes (Coleman *et al*., 1965; Taylor & Neal, 1989). These classifications are based on distinct eclogite suites from Southern African kimberlites and do not necessarily reflect the particularities of eclogites from other localities. We therefore use a slightly different scheme ('types' in Table 1) that reflects the specific groupings of eclogites in this study with regard to Cr_2O_3–CaO, CaO/(MgO + FeO)–MgO/FeO and CaO–Na_2O relationships in garnet (see below).

Garnet modes in volatile-free eclogites range from ~40 to 90 vol. % and cpx modes from ~10 to 55%, with an average and median garnet mode of ~60% and 65%, respectively. Two samples have high modal amounts of phlogopite (44 and 48%, respectively) in addition to garnet and cpx and are therefore not eclogites *sensu stricto*

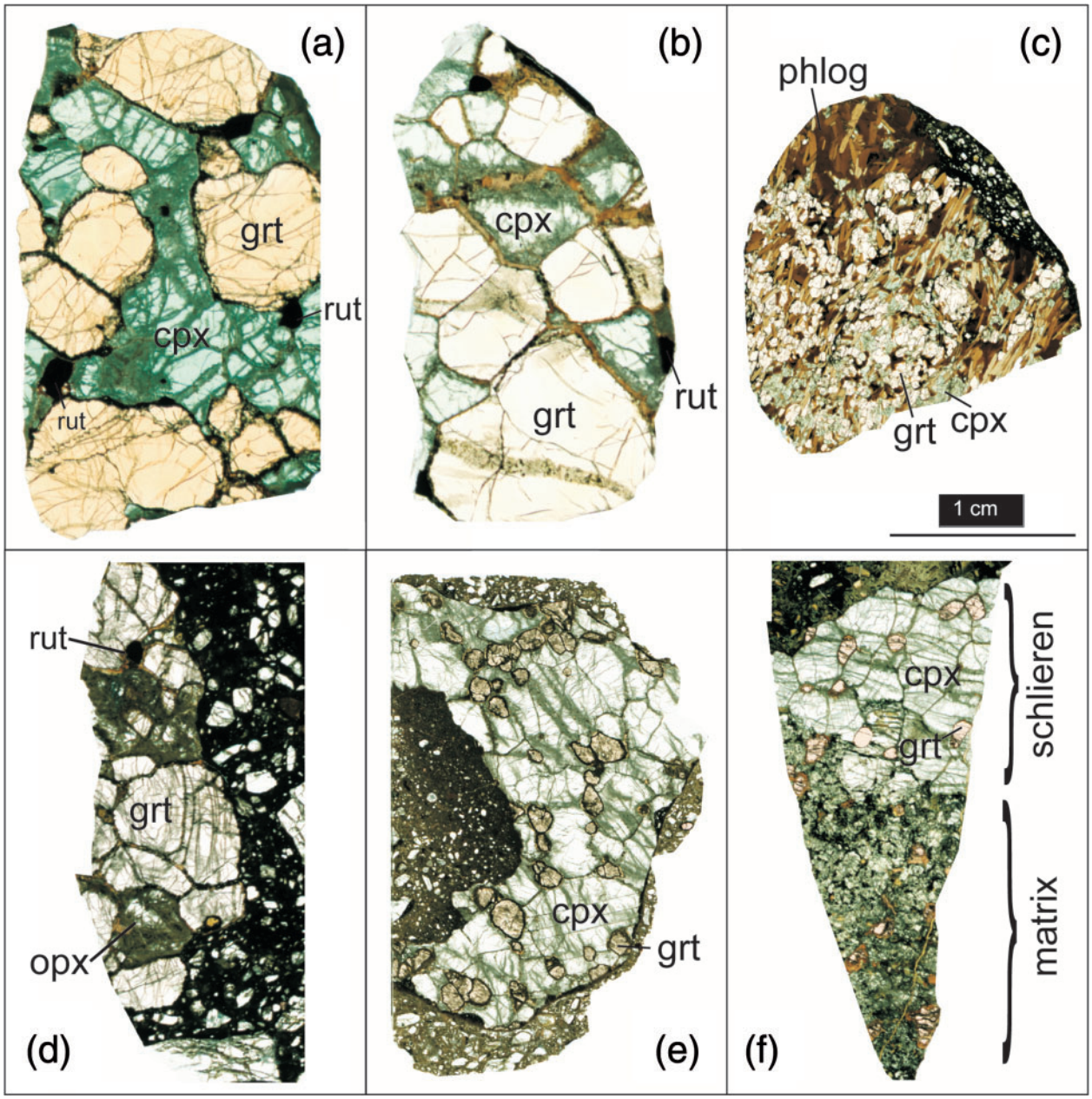

Fig. 2. Eclogites in thin section (plane-polarized light) illustrating the microstructures mentioned in the text: (a) high-Mg eclogite VR67360; (b) high-Mg eclogite YK1946; (c) phlogopitized eclogite YK1911; (d) garnet pyroxenite YK1915; (e) garnet pyroxenite YK1914; (f) garnet pyroxenite schlieren in a matrix of garnet, spongy opx and glass (YK1952). Grt, garnet; cpx, clinopyroxene; rut, rutile; phlog, phlogopite. Scalebar in (c) applies to all sections (1 cm).

(phlogopite occurring as small secondary grains at grain boundaries and in veins is not considered in this study). Ten samples of all eclogite types show secondary spongy rims of cpx around cpx cores. Secondary rims contain small (μm-scale) patches of glass.

Rutile is the most common primary accessory phase (15 of 65 eclogites and pyroxenites) with modes between <1 and 2 vol. %. Sulfide occurs in 14 samples and is present as rounded to subhedral to irregular grains. Kyanite has been identified in three samples studied by Pearson *et al.* (1999). One of the kyanite-bearing eclogites also contains diamond (VR40345). Kyanite, as well as diamond or graphite associated with kyanite-bearing and compositionally similar eclogites (high-Ca eclogites), has been frequently observed in drill core (Pearson *et al.*, 1999), but because these eclogite types are often altered and friable, they are not proportionally represented in the present study. One high-Ca eclogite (VR43465) contains

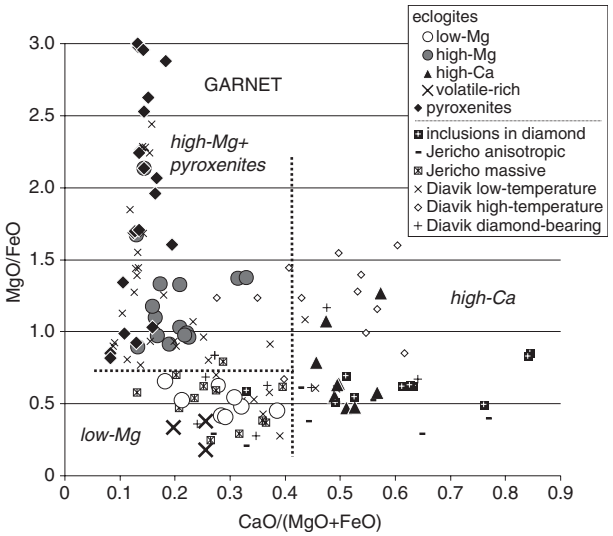

Fig. 3. CaO/(MgO + FeO) vs MgO/FeO (wt %) in garnet. Fields distinguish low-Mg and high-Ca eclogites as well as high-Mg eclogites plus pyroxenites in this study. Garnets in eclogites from Jericho (Kopylova *et al.*, 1999) and Diavik (Schmidberger *et al.*, 2007) are shown for comparison. Garnet inclusions in diamond from Davies *et al.* (1999, 2004).

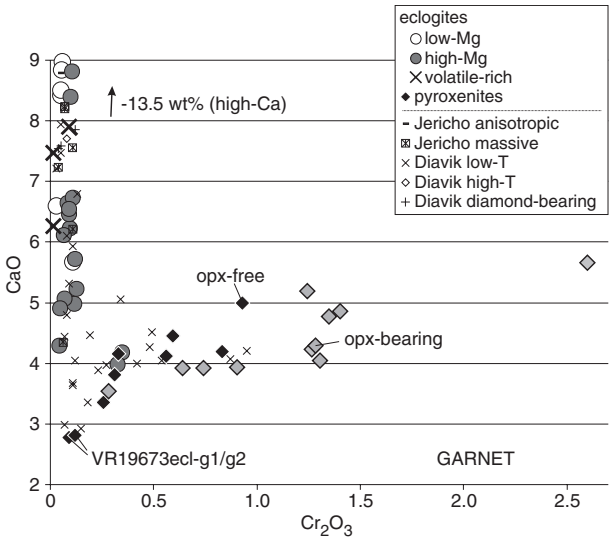

Fig. 4. Cr_2O_3 vs CaO (wt %) in garnet. Garnets in eclogites from Jericho and Diavik as in Fig. 3.

3 vol. % graphite, which occurs as disseminated plates several millimetres long with prismatic tabular or irregular habit. Quartz has been retrieved from a mineral separate of low-Mg eclogite YK1943. The phlogopitized samples (VR19674ecl-g7 and YK1911) also contain apatite and glass as accessory phases. Vesicles in sample VR67112b are partially filled with single or multiple large carbonate crystals.

Most pyroxenites from Lac de Gras have fine- to coarse-grained granoblastic equilibrated microstructures (Pearson *et al.*, 1999). Modal information for pyroxenites in the present study is available for only the larger sample YK1914 (22% garnet, 78% cpx) (Fig. 2e).

MAJOR ELEMENTS

Average major-element compositions of garnet, cpx and opx in the different eclogite types (except for the three volatile-rich eclogites which are not averaged) and in pyroxenites are given in Table 2; the full datasets, including accessory minerals, are available as Electronic Appendices 2–5, which can be downloaded from http://petrology.oxfordjournals.org.

Garnet

Garnets have X_{Mg} [pyrope component: 100Mg/(Mg + Fe + Ca + Mn)] ranging from 17·8 to 75·6 and X_{Ca} (grossular component; mol%) ranging from 7·2 to 35·9 (Electronic Appendix 2). In a diagram of CaO/(MgO + FeO) vs MgO/FeO (Fig. 3), eclogitic garnets fall into three groups: (1) low-Mg: garnets with low CaO/(MgO + FeO) and low MgO/FeO; (2) high-Mg: garnets with low CaO/(MgO + FeO) and high MgO/FeO; (3) high-Ca: those with high CaO/(MgO + FeO) and intermediate MgO/FeO. Volatile-rich eclogites have garnets with the lowest MgO/FeO, whereas pyroxenites trend towards higher values than eclogites.

Most eclogite garnets have Cr_2O_3 contents <0·2 wt % with variable CaO contents (Fig. 4). Garnets in pyroxenites have low CaO contents, which correlate positively with Cr_2O_3. More than half of the pyroxenites are opx-free and all pyroxenites are olivine-free on thin-section scale. Pyroxenitic garnets show an opposing trend of CaO vs Na_2O (Fig. 5) compared with the eclogitic garnets. Because the positive correlation of Cr_2O_3 and CaO for pyroxenitic garnet indicates buffering by both cpx and opx, opx-bearing or opx-free pyroxenites will not be further distinguished subsequently (except in the geothermobarometry section where opx-bearing assemblages allow simultaneous calculation of pressure and temperature).

Distinct rim compositions in most garnets are characterized by lower CaO contents and higher Mg-number [= 100Mg/(Mg + Fe)]. Garnet compositions in three samples are inhomogeneous with regard to CaO, MgO and FeO (SE01, VR43479 and VR43480) without clear core–rim zonations, similar to coexisting cpx. Like rims, CaO-poor compositions are characterized by higher Mg-number. Visibly secondary spongy cpx rims also have higher MgO contents (see below), and MgO-rich garnets are, therefore, regarded as affected by secondary changes.

Based on Cr–Ca, Mg–Ca–Fe and Ca–Na compositional relationships in garnet, the following eclogite types are distinguished: (1) eclogites with high-Ca

Table 2: Summary of major-element contents in garnet and cpx (wt %)

	SiO_2	TiO_2	Al_2O_3	Cr_2O_3	FeO^{total}	MnO	MgO	CaO	Na_2O	Total	Mg-no.	*T*(Krogh)	Type
Garnet													
Low-Mg ecl	39·64	0·26	22·14	0·11	18·43	0·37	10·50	8·46	0·09	100·0	50·3	976	
minimum	38·93	0·08	21·30	<0·09	10·71	0·24	8·49	5·67	0·06	99·0	42·3	860	
maximum	40·94	0·36	22·75	0·11	20·93	0·46	14·57	10·62	0·12	100·4	70·8	1088	
1σ	0·70	0·12	0·52	n.a.	3·54	0·07	2·27	1·85	0·03	0·5	9·9	98	
High-Mg ecl	40·81	0·26	22·61	0·13	14·19	0·30	15·37	6·24	0·07	100·0	65·9	969	
minimum	39·70	0·08	22·24	<0·09	9·51	0·23	11·27	4·18	0·03	99·1	55·1	820	
maximum	42·50	0·52	23·23	0·35	17·95	0·36	20·30	8·82	0·13	101·2	79·2	1241	
1σ	0·77	0·13	0·31	n.a.	2·25	0·04	1·89	1·41	0·03	0·5	5·7	88	
High-Ca ecl	39·79	0·34	22·11	n.a.	15·16	0·27	9·58	12·40	0·11	99·8	52·8	1078	
minimum	39·09	0·11	21·17	<0·09	11·64	0·23	8·01	11·44	0·07	98·9	45·6	910	
maximum	40·39	0·73	22·42	0·11	17·13	0·35	12·49	13·51	0·18	100·4	65·7	1246	
1σ	0·42	0·26	0·42	n.a.	1·73	0·04	1·55	0·73	0·04	0·6	6·7	151	
vr19674ecl-g7	38·67	0·03	21·87	<0·09	23·80	1·53	7·93	6·27	<0·04	100·2	37·3		volatile-rich
vr67112b	37·83	0·13	20·97	0·09	26·20	2·04	4·66	7·90	<0·04	99·9	24·1		volatile-rich
yk1911	38·74	<0·06	22·00	<0·09	21·20	2·21	8·02	7·47	<0·04	99·7	40·3		volatile-rich
Pyroxenites	41·63	0·21	22·57	0·75	11·48	0·34	19·06	4·07	0·06	100·2	74·7	909	
minimum	39·89	0·05	20·81	0·09	7·29	0·25	15·35	2·77	0·04	99·6	59·3	699	
maximum	42·79	0·48	23·30	2·60	18·81	0·54	22·15	5·66	0·09	101·1	84·2	1158	
1σ	0·68	0·10	0·57	0·57	3·23	0·07	2·09	0·65	0·01	0·4	7·3	117	

	SiO_2	TiO_2	Al_2O_3	Cr_2O_3	FeO^{total}	MnO	MgO	CaO	Na_2O	Total	Mg-no.	Type
Cpx												
Low-Mg ecl	54·53	0·28	7·39	n.a.	5·00	<0·09	11·17	16·62	4·34	99·4	80·1	
minimum	51·60	0·17	5·64	<0·09	3·37	n.a.	8·76	13·88	1·97	98·1	74·1	
maximum	55·70	0·44	10·67	0·14	6·87	n.a.	13·24	19·26	6·32	100·1	86·5	
1σ	1·28	0·11	1·55	n.a.	1·24	n.a.	1·53	1·77	1·26	0·6	4·0	
High-Mg ecl	54·83	0·23	4·83	n.a.	3·81	n.a.	13·68	18·75	3·18	99·4	86·5	
minimum	53·53	0·09	2·63	<0·09	2·45	<0·09	11·56	16·17	2·04	98·6	77·8	
maximum	56·45	0·31	8·10	0·16	6·74	0·11	15·88	21·01	4·95	101·1	92·0	
1σ	0·71	0·07	1·37	n.a.	0·95	n.a.	1·04	1·38	0·75	0·6	3·0	
High-Ca ecl	55·63	0·27	11·84	n.a.	3·18	<0·09	8·68	13·68	6·15	99·5	83·6	
minimum	54·48	0·14	7·69	<0·09	1·68	n.a.	6·19	10·60	3·91	98·7	75·1	
maximum	56·70	0·49	15·79	0·10	6·03	n.a.	11·48	16·89	8·07	100·3	87·8	
1σ	0·76	0·15	3·34	n.a.	1·51	n.a.	1·89	2·61	1·67	0·6	4·5	
vr19674 ecl-g7	53·22	0·10	1·85	<0·09	5·36	0·15	14·48	23·39	0·62	99·2	82·8	volatile-rich
vr67112b	50·40	0·41	3·28	<0·09	10·79	0·24	11·08	22·29	0·71	99·2	64·7	volatile-rich
yk1911	52·31	0·14	3·01	<0·09	5·44	0·24	14·50	23·40	0·56	99·6	82·6	volatile-rich
Pyroxenites	55·27	n.a.	3·47	0·38	3·04	n.a.	15·43	19·59	2·45	99·9	89·9	
minimum	52·99	<0·06	0·37	0·10	1·49	<0·09	11·28	14·08	0·30	99·0	80·4	
maximum	56·66	0·37	7·86	1·34	4·90	0·14	18·63	23·12	5·37	100·9	94·7	
1σ	0·68	n.a.	1·89	0·28	0·91	n.a.	1·93	2·26	1·31	0·5	3·7	

	SiO_2	TiO_2	Al_2O_3	Cr_2O_3	FeO^{total}	MnO	MgO	CaO	NiO	Total	Mg-no.
Opx											
Pyroxenites	57·81	n.a.	0·59	n.a.	6·27	n.a.	35·08	0·37	0·11	100·6	90·9
minimum	55·46	<0·06	0·32	<0·09	4·62	<0·09	29·99	0·20	0·08	99·6	80·4
maximum	58·88	0·09	3·18	0·54	13·04	0·14	36·28	0·77	0·14	101·4	93·3
1σ	0·98	n.a.	0·67	n.a.	2·12	n.a.	1·60	0·19	0·02	0·6	3·2

Averaged for the three eclogite types and for pyroxenites; minimum and maximum values as well as standard deviations also given. Concentrations in volatile-rich eclogites are shown individually; ecl, eclogite, Mg-number = 100Mg/(Mg + Fe). Temperatures of last equilibration [*T*(Krogh)] as in Electronic Appendix 8.

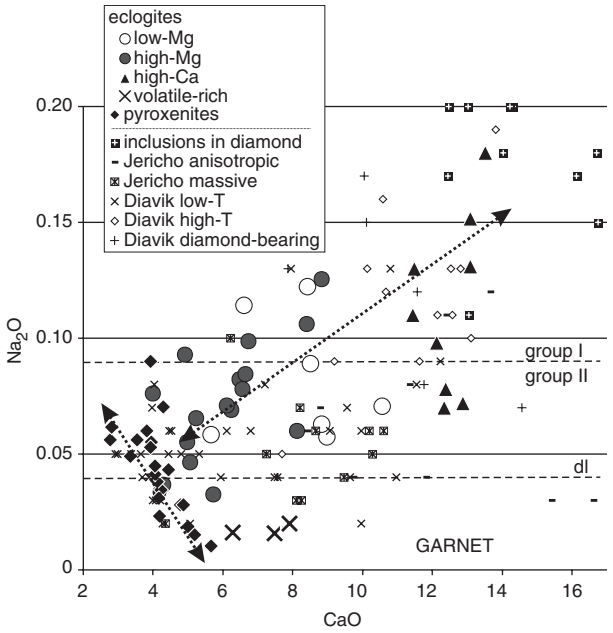

Fig. 5. CaO vs Na_2O (wt %) in garnet. Arrows show trends for eclogites and pyroxenites, respectively [note that part of the pyroxenite trend extends into the field falling below the detection limit (dl) for Na_2O]. Group I and group II refer to classification of McCandless & Gurney (1989). Data sources as in Figs 3 and 4.

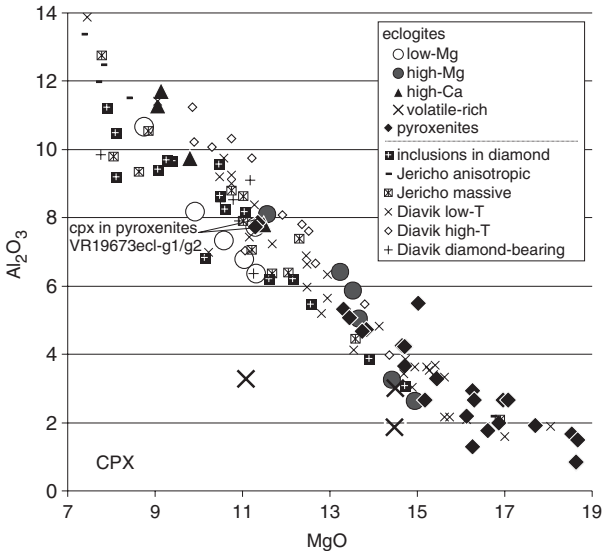

Fig. 6. MgO vs Al_2O_3 (wt %) in cpx. Data sources as in Figs 3 and 4.

garnets (these include kyanite-, graphite- and diamond-bearing varieties); (2) eclogites with low-Mg garnets (these include quartz-bearing eclogite); (3) eclogites with high-Mg garnets and Cr_2O_3 contents $<0{\cdot}2$ wt %; (4) volatile-rich eclogites (phlogopite-, apatite-, carbonate-bearing).

Clinopyroxene (cpx)

Clinopyroxenes in all eclogite groups have higher average Al_2O_3 contents than those in pyroxenites, with the former having about 90% of the total Al in the jadeite molecule (Al^{VI}), versus about 35% for the latter, corresponding to an average of 4·1 and 2·5 wt % Na_2O, respectively. The highest Al_2O_3 and Na_2O contents in the dataset are observed in cpx from the high-Ca eclogites (up to 15·8 wt % Al_2O_3) (Electronic Appendix 3). Contents of K_2O are generally below the detection limit ($<0{\cdot}04$ wt %), but values up to 0·24 wt % are observed in some cpx in high-Ca eclogites. Average cpx Mg-number are highest in pyroxenites (89·9), followed by cpx in high-Mg eclogites (86·5), high-Ca eclogites (83·6) and low-Mg eclogites (80·1). Pyroxenitic cpx tend to have lower TiO_2 and higher NiO and distinctly higher Cr_2O_3 contents compared with those in eclogites. A plot of MgO vs Al_2O_3 shows a negative correlation (Fig. 6). Clinopyroxenes in low-Mg eclogites have lower Al_2O_3 contents at a given MgO content than other eclogite types. Between ~15 and 17 wt % MgO, the Al_2O_3–MgO correlation for cpx in pyroxenites has a different slope from that in the eclogites. Clinopyroxenes in pyroxenites VR19673ecl-g1 and VR19673ecl-g2 have distinctly lower MgO contents and higher Al_2O_3 contents than in the other pyroxenites. They coexist with garnets having the lowest Cr_2O_3 and CaO contents of the dataset, which define one end of the positive Cr_2O_3–CaO correlation observed for garnets.

Clinopyroxenes in volatile-rich eclogites have distinctly high MnO contents (up to 0·24 wt %); Mg-numbers for cpx in the phlogopite-bearing variety are 82·6 and 82·8, whereas that in the calcite-bearing eclogite (VR67112b) has an Mg-number of 64·7.

Some cpx grains have spongy rims that contain small (μm-scale) patches of glass; these rims are richer in Ca and Mg and markedly poorer in Na than the cores, similar to cpx in eclogites from southern Africa (Taylor & Neal, 1989). The rim texture is unequilibrated, suggesting late growth. The formation of the spongy cpx rims might be related to incongruent melting of cpx, or be a result of metasomatism (Taylor & Neal, 1989, and references therein). Distinct, although not spongy, rims in two eclogites (VR67360 and YK1946) are similarly enriched in CaO and depleted in Na_2O. Two types of cpx with respect to CaO, Na_2O and Mg# are present in VR43477, VR43479 and VR43480, without clear core–rim zonation or spongy rims. No significant differences are recognized with respect to other oxides.

Orthopyroxene (opx)

Orthopyroxenes have Mg-number ranging from 80·4 to 93·3 (17 of 19 samples have values between 89·5 and 93·3) and typically contain minor amounts of Al_2O_3 (0·32–1·18 wt %; one outlier has 3·18 wt %), CaO (0·20–1·18 wt %) and NiO (0·08–0·14 wt %) (Electronic

Appendix 4). The contents of all other elements are mostly below their respective detection limits.

Accessory phases

Rutile and ilmenite occur in some of the eclogites (Table 1). All rutile grains have exsolved ~10% ilmenite as lamellae and rims. Ilmenite-free areas of rutile in eclogites contain between 96·2 and 98·8 wt % TiO_2 and minor amounts of Al_2O_3 (0·1–0·4 wt %), Cr_2O_3 (<0·09 to 0·2 wt %) and FeO (0·3–0·7 wt %). Rutile in pyroxenite YK1915 contains 0·04 wt % Al_2O_3, 0·1 wt % FeO, and 1·5 wt % Cr_2O_3. Discrete ilmenite grains in sample VR67112b have TiO_2 contents of 49·9 and 50·0 wt %, MgO of 2·3 and 1·5 wt %, and FeO of 39·9 and 40·3 wt %, respectively.

Sulfides occur interstitially or enclosed in cpx, garnet and opx; they are mostly pyrrhotite and monosulfide solid solution with variable Ni contents (unpublished data). They will not be considered further here.

Abundant platy phlogopite is observed in two samples (VR19674ecl-g7 and YK1911). It is Cl-rich in sample VR19674ecl-g7 (0·63 wt % vs 0·03 wt % in YK1911) and F-rich in sample YK1911 (0·97 wt % vs 0·05 wt % in VR19674ecl-g7) (Electronic Appendix 5). The same is true for coexisting apatite (VR19674ecl-g7: 2·54 wt % Cl and 0·14 wt % F; YK1911: 0·06 wt % Cl and 3·06 wt % F).

Comparison with mineral inclusions in diamonds from Lac de Gras and with eclogite xenoliths from other Slave Craton localities

Mineral inclusions in diamonds from the Lac de Gras kimberlites have been investigated by Davies *et al.* (1999, 2004). For garnets, there is a striking similarity between the inclusions in diamond and those in the high-Ca eclogite xenoliths, although the inclusions in diamond trend towards higher Na_2O (Fig. 5) and lower Al_2O_3 contents. The overlap is not as marked for cpx, where inclusions in diamond span almost the entire range observed for eclogitic cpx (Fig. 6).

A comparison with eclogites from other localities in the Slave Craton shows that garnets in most Diavik low-temperature eclogites reported by Schmidberger *et al.* (2007) plot with garnets in high-Mg eclogites and in pyroxenites from this study (Figs 3–5), whereas garnets in high-temperature and diamond-bearing eclogites (Schmidberger *et al.*, 2007) overlap most with garnets in high-Ca eclogites from this study and with garnets included in diamond. Eclogites from the Jericho kimberlite have either massive or anisotropic fabrics (Kopylova *et al.*, 1999). Garnets in almost all massive eclogites plot with garnets in low-Mg eclogites from this study with regard to CaO–MgO–FeO relationships (Fig. 3), but many have lower Na_2O contents at a given CaO content (Fig. 5). Garnets in anisotropic eclogites are restricted to low MgO/FeO (<0·7) and show some overlap with garnets in high-Ca eclogites although trending towards lower CaO/(MgO + FeO) (Fig. 3), while coexisting cpx is also restricted to low MgO and trends toward high Al_2O_3 contents (Fig. 6).

TRACE ELEMENTS

Garnet

Trace-element abundances in garnet are summarized in Table 3 and the complete dataset is reported in Electronic Appendix 1. Garnets in low-Mg eclogites show steep positive slopes between La_N and Sm_N and shallower positive slopes in the normalized heavy rare earth elements ($HREE_N$; Fig. 7a). The normalized light REE ($LREE_N$) show an order of magnitude variability. Zr/Hf is mostly supra-chondritic and Ti can be enriched or depleted relative to elements of similar compatibility. Niobium in three samples is strongly depleted at 0·02–0·03 × chondritic. Garnets in high-Mg eclogites also show smooth positive slopes in $LREE_N$ but have flat $HREE_N$ and variable normalized middle REE ($MREE_N$) to $HREE_N$ (Fig. 7b). Zr/Hf is always supra-chondritic and Ti enriched or depleted relative to similarly compatible elements. Niobium is most samples is below detection. Small positive Eu anomalies, though not outside the analytical uncertainty for Eu relative to either Sm or Gd, are observed for garnet in some high-Mg eclogites (e.g. Eu/Eu^* up to 1·5, for VR67360, where Eu^* is the average of the chondrite-normalized Sm and Gd concentrations). Garnets in high-Ca eclogites are slightly enriched in the $MREE_N$ relative to the $HREE_N$, or have flat $MREE_N$ and $HREE_N$ with a hump between Eu_N and Ho_N (Fig. 7c). One sample (VR40345) shows strong La enrichment (greater than chondrite). Two samples have supra-chondritic Zr/Hf whereas three samples have close to chondritic ratios and one sample has a subchondritic ratio. As is true for the other eclogite types, Ti_N is either enriched or depleted relative to similarly compatible elements.

Pyroxenitic garnets have variable slopes in the $LREE_N$, and flat $MREE_N$ to $HREE_N$ patterns, and two samples show high Sc relative to neighbouring elements. Garnet in one of the pyroxenites (YK1952) has a highly distinctive pattern relative to other pyroxenites, with very low LREE and HFSE (Fig. 7d). This sample consists of coarse pyroxenite schlieren, in which the garnet was analysed, in a finer-grained 'matrix' of spongy cpx with secondary rims, fine cpx–opx intergrowths, embayed garnet and melt patches.

Volatile-rich eclogites have garnets that are slightly enriched in $MREE_N$ relative to $HREE_N$ or have flat MREE to HREE patterns. One garnet has a pronounced negative Eu anomaly ($Eu/Eu^* = 0·7$, for VR67112b; Fig. 7e). Garnets in volatile-rich samples have the lowest Ni, Co and Ti, and the highest V, Sc, Y and HREE abundances in the dataset.

Table 3: Summary of trace-element contents in garnet and cpx (ppm)

	Cpx																		
Type:	Low-Mg				High-Mg				High-Ca				volatile-rich		Pyx				
	av.	min.	max.	1σ	av.	min.	max.	1σ	av.	min.	max.	1σ	VR19674 ecl-g7	VR67112b	YK1911	av.	min.	max.	1σ
n:	6				6				7				3	5	4	4			
P	169	54	270	88	196	70	310	78	282	80	450	138	160	60	80	214	48	370	144
Sc	62	40	89	16	48	36	67	11	53	42	79	15	69	92	93	186	52	440	179
Ti	1667	490	2500	680	1073	620	2000	455	2141	700	4700	1582	270	690	260	1097	540	1900	573
V	169	78	250	68	150	78	280	72	178	110	390	101	140	340	100	390	71	820	326
Co	59	42	70	11	58	39	84	13	58	47	65	5	30	41	27	68	55	90	16
Ni	17	5	32	10	21	11	34	10	24	11	35	8	6	1·0	<1	54	25	110	38
Ga	12	7	15	3	13	8	16	3	12	9	20	4	8	8·6	5·8	12	10	14	2
Sr	n.a.	<1·2	4	n.a.	n.a.	<2·2	<2·2	n.a.	n.a.	<7	<7	n.a.	<2	<0·25	<1·0	<1·3	<1·3	<1·3	n.a.
Y	37	6	61	18	21	7	38	10	31	20	38	5	60	81	70	19	12	26	6
Zr	15	5	29	9	28	6	83	26	24	9	43	12	60	22	90	18	1	41	17
Nb	0·09	0·005	0·48	0·19	n.a.	<0·015	0·5	n.a.	n.a.	<0·05	0·5	n.a.	<0·03	0·012	<0·01	0·22	0·030	0·57	0·25
La	0·05	0·01	0·09	0·04	n.a.	<0·007	0·0	n.a.	n.a.	<0·03	0·4	n.a.	0·04	0·02	0·009	0·03	0·00	0·09	0·05
Ce	0·3	0·1	0·5	0·2	0·1	0·0	0·1	0·0	0·5	0·1	1·8	0·5	0·3	0·22	0·15	0·1	0·0	0·3	0·1
Pr	0·1	0·0	0·2	0·1	0·0	0·0	0·1	0·0	0·2	0·1	0·3	0·0	0·17	0·14	0·12	0·0	0·0	0·1	0·0
Nd	1·2	0·3	2·4	0·7	0·7	0·4	1·4	0·3	2·1	1·2	3·2	0·7	2·4	2·3	2·0	0·3	0·0	0·7	0·3
Sm	1·1	0·4	2·2	0·6	1·0	0·3	1·8	0·5	2·3	0·8	3·6	1·0	2·9	3·1	3·3	0·5	0·1	0·9	0·4
Eu	0·6	0·3	1·0	0·3	0·6	0·2	1·0	0·3	1·1	0·4	1·7	0·4	1·6	1·14	1·6	0·3	0·1	0·6	0·2
Gd	2·7	0·7	4·1	1·2	2·3	0·7	4·2	1·2	4·3	1·6	5·3	1·3	8	8·1	9·0	1·3	0·6	2·4	0·8
Dy	5·4	1·1	7·0	2·3	3·6	1·3	6·5	1·8	5·8	3·5	7·1	1·1	12	14·4	12	2·9	1·8	4·2	1·0
Ho	1·4	0·2	2·3	0·7	0·8	0·3	1·5	0·4	1·2	0·9	1·4	0·2	2·4	3·0	2·3	0·7	0·4	1·0	0·2
Er	4·6	0·7	8·0	2·4	2·4	0·9	4·0	1·0	3·4	2·5	4·0	0·5	8	8·5	6	2·2	1·4	2·8	0·6
Yb	5·2	0·6	9·8	3·0	2·4	1·0	3·7	0·8	3·2	2·2	3·9	0·5	8	7·0	5	2·3	1·3	3·0	0·7
Lu	0·9	0·1	1·6	0·5	0·4	0·2	0·5	0·1	0·5	0·3	0·7	0·1	1·1	0·9	0·8	0·4	0·2	0·5	0·1
Hf	0·3	0·2	0·5	0·1	0·4	0·1	1·0	0·3	0·5	0·2	0·9	0·2	0·9	0·27	0·07	0·3	0·0	0·6	0·3
Ta	n.a.	<0·008	<0·04	n.a.	n.a.	<0·005	0·01	n.a.	n.a.	<0·004	n.a.	n.a.	0·03	<0·002	<0·005	n.a.	<0·007	0·11	n.a.
Pb	n.a.	<0·05	0·2	n.a.	n.a.	<0·02	0·2	n.a.	n.a.	<0·03	0·7	n.a.	0·2	0·04	<0·02	n.a.	<0·03	0·1	n.a.
Th	n.a.	<0·01	0·05	n.a.	n.a.	<0·007	0·03	n.a.	n.a.	<0·008	0·11	n.a.	<0·07	0·012	<0·004	0·02	0·005	0·06	0·02
U	n.a.	<0·03	<0·03	n.a.	n.a.	<0·01	0·1	n.a.	n.a.	<0·07	n.a.	n.a.	0·1	0·023	0·10	n.a.	<0·01	0·03	n.a.

	Cpx																		
Type:	Low-Mg				High-Mg				High-Ca				volatile-rich		Pyx				
	av.	min.	max.	1σ	av.	min.	max.	1σ	av.	min.	max.	1σ	VR67112b	YK1911	av.	min.	max.	1σ	
n:	6				4				8				5	4	4				
P	65	15	120	41	39	14	56	16	53	30	70	12	20	9	80	27	120	40	
Sc	22	10	30	7	15	14	19	2	14	7	24	5	80	43	17	11	21	5	
Ti	1557	990	2400	508	1168	1010	1490	191	1988	810	3500	1154	2390	1700	689	102	1685	694	
V	415	180	480	107	318	210	400	69	324	259	450	72	600	180	250	139	480	156	
Co	35	26	50	8	20	14	31	7	26	14	42	11	49	23	29	20	42	10	
Ni	164	87	220	47	228	100	430	128	188	135	320	56	59	34	428	410	670	184	

(continued)

Table 3: Continued

	Cpx																	
Type:	Low-Mg				High-Mg				High-Ca				volatile-rich		Pyx			
	av.	min.	max.	1σ	av.	min.	max.	1σ	av.	min.	max.	1σ	VR67112b	YK1911	av.	min.	max.	1σ
n:	6				4				8				5	4	4			
Ga	16	10	20	3	12	9	15	2	26	15	39	9	12·9	12·3	6	1·1	11	5
Rb	n.a.	<0·08	0·4	n.a.	n.a.	<0·07	0·5	0·2	n.a.	<0·03	0·3	n.a.	0·2	<0·04	0·3	0·10	0·5	0
Sr	166	85	290	74	222	153	285	50	243	83	440	142	8·5	12·0	200	1·1	414	209
Y	2	0·4	4	1·0	1·3	0·7	2	0·4	1·1	0·3	3	1·0	2·8	5·1	2	0·3	3	2
Zr	19	4	48	15	25	8	45	13	17	8	28	7	111	129	36	0·08	81	42
Nb	0·1	0·003	0·3	0·1	n.a.	<0·02	0·0	n.a.	n.a.	<0·02	16	9	0·07	0·11	0·10	0·03	0·2	0·08
Cs	n.a.	<0·01	6	n.a.	n.a.	<0·06	<0·06	n.a.	<0·13	<0·04	<0·13	n.a.	b.d.l.	<0·02	n.a.	<0·01	<0·02	n.a.
Ba	0·9	0·2	2	0·7	0·9	0·1	2	0·7	1·0	0·3	3	1·0	0·6	0·1	1·3	0·6	3	1·0
La	3	0·3	8	3	3	2·3	3	0·4	4	0·1	14	6	5·1	9·7	4	0·1	10	4
Ce	7	1·3	20	6	10	7	13	2	7	0·5	24	10	25	28	11	0·1	28	13
Pr	1·1	0·2	3	0·8	2	1·0	3	0·6	0·8	0·2	2	0·9	4·7	4·6	2	0·02	4	2
Nd	5	1·2	12	4	10	5	14	4	4	0·9	8	2·6	23	22	8	0·1	22	10
Sm	1·1	0·5	2·1	0·6	2·0	1·0	3·1	1·0	0·7	0·2	1·1	0·3	4·7	5·3	2	0·05	5	2
Eu	0·3	0·1	0·5	0·1	0·6	0·28	0·9	0·3	0·2	0·10	0·3	0·07	0·87	1·23	0·6	0·02	1·5	0·7
Gd	0·8	0·3	1·3	0·3	1·1	0·5	1·9	0·6	0·5	0·3	0·6	0·11	2·8	3·7	1·5	0·10	3·6	2
Dy	0·5	0·1	0·7	0·2	0·4	0·22	0·6	0·1	0·2	0·13	0·3	0·07	1·1	1·6	0·7	0·08	1·4	0·6
Ho	0·1	0·0	0·2	0·04	0·06	0·03	0·07	0·02	n.a.	<0·03	0·12	n.a.	0·11	0·21	0·09	0·01	0·2	0·07
Er	n.a.	<0·7	<0·7	n.a.	0·11	0·04	0·2	0·0	n.a.	<0·06	0·3	n.a.	0·19	0·33	0·2	0·02	0·3	0·12
Yb	n.a.	<0·01	0·2	n.a.	n.a.	<0·01	0·11	n.a.	n.a.	<0·06	0·3	n.a.	0·07	0·15	0·09	0·01	0·2	0·06
Lu	n.a.	<0·01	0·03	n.a.	n.a.	<0·002	0·02	n.a.	n.a.	<0·008	0·1	n.a.	0·006	0·013	0·013	0·002	0·03	0·01
Hf	1·2	0·3	2·4	0·7	1·1	0·4	1·8	0·5	1·0	0·6	1·6	0·4	3·4	5·3	n.a.	<0·015	3·5	n.a.
Ta	n.a.	<0·003	<0·015	n.a.	n.a.	<0·006	0·06	n.a.	n.a.	<0·004	<0·04	n.a.	0·014	0·0236	n.a.	<0·003	<0·3	n.a.
Pb	0·6	0·2	1·2	0·4	0·6	0·4	0·9	0·2	n.a.	<0·16	0·7	0·2	0·65	0·98	0·8	0·1	1·8	1
Th	n.a.	<0·005	0·6	n.a.	0·12	0·05	0·2	0·05	n.a.	<0·02	<0·06	n.a.		0·21	0·2	0·01	0·6	0·3
U	n.a.	<0·05	<0·05	n.a.	0·02	0·009	0·05	0·01	n.a.	<0·03	<0·05	n.a.	0·013	0·24	n.a.	<0·005	0·03	n.a.

Averaged for the three eclogite types and for pyroxenites, as in Table 2; pyx, pyroxenite, *n*, number of analyses averaged; b.d.l., below detection limit.

Clinopyroxene

Trace-element abundances in cpx are summarized in Table 3 and the complete dataset is reported in Electronic Appendix 6. Clinopyroxenes in low-Mg eclogites have mildly positive to negative slopes from La_N to Nd_N, and smooth negative slopes between Sm_N and Ho_N that mostly continue to Lu_N (Fig. 8a). Niobium is below detection or <0·07 chondritic and Sr_N is variably enriched relative to neighbouring elements, with the peak size correlating negatively with $LREE_N$. Zr/Hf is subchondritic and Hf_N is enriched relative to Sm_N, whereas Ti_N is enriched or depleted relative to similarly compatible elements. We analysed the spongy rim in cpx YK1943 and its trace-element pattern is similar to that of cpx cores for more compatible elements whereas the most incompatible elements are several orders of magnitude higher. Clinopyroxenes in high-Mg eclogites have steeper negative slopes between Nd_N and Lu_N than those in low-Mg eclogites, combined with lower HREE abundances; Hf_N is depleted relative to Sm_N (Fig. 8b) High-Ca eclogites contain cpx with sinusoidal REE_N patterns with lower LREE than other eclogite types and the heaviest REE below detection. They have uniformly strong positive Sr peaks relative to elements of similar compatibility (Fig. 9). The diamond-bearing high-Ca eclogite (VR40345) has cpx with unusually high Nb and LREE abundances.

Clinopyroxenes in four pyroxenites have disparate trace element patterns. They all share depletions in Ti_N relative to similarly compatible elements and two show positive Sr_N peaks. Two samples have cpx with high and flat $LREE_N$ to $MREE_N$ patterns and steep negative slopes in the $HREE_N$. The trace-element patterns of cpx in YK1914

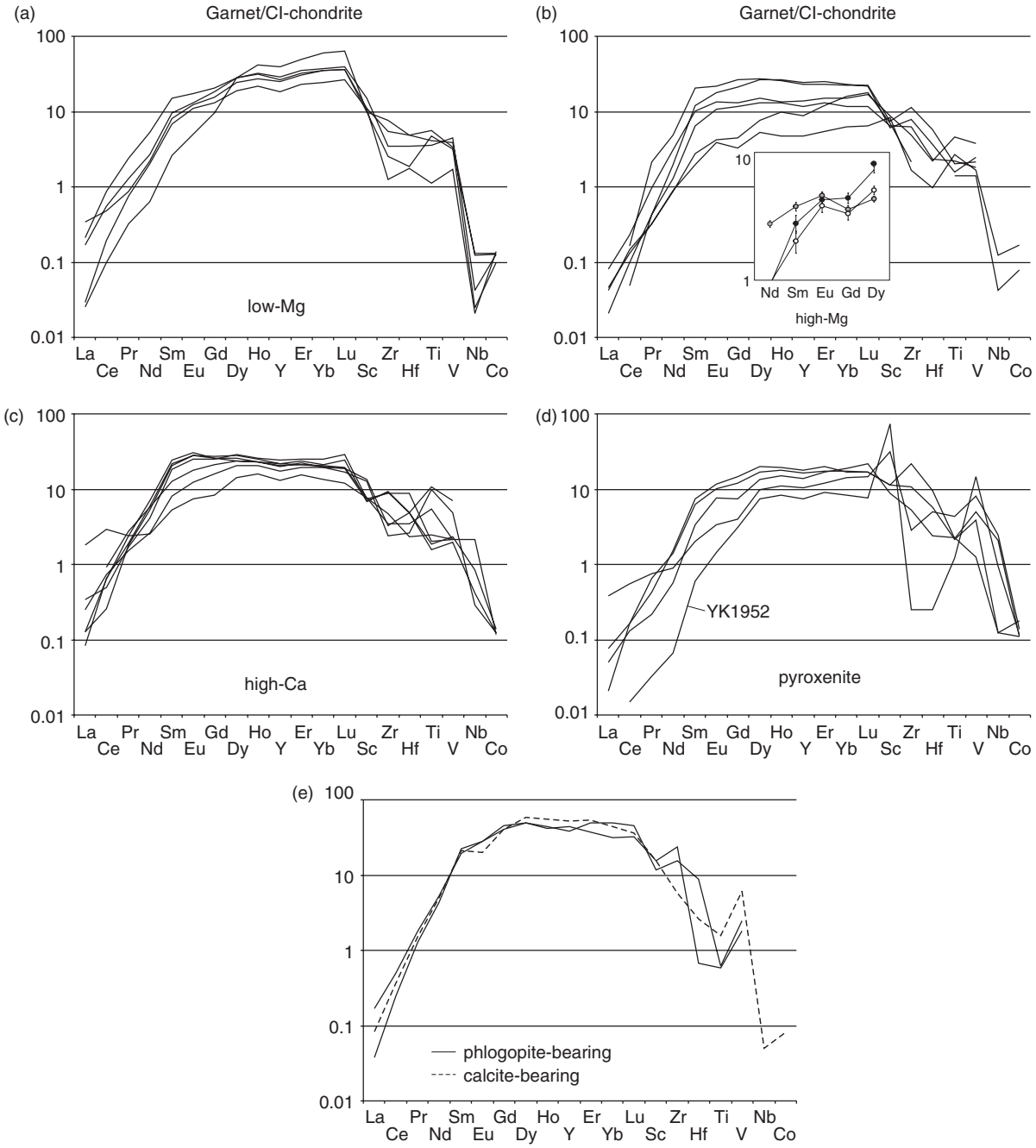

Fig. 7. Extended trace-element patterns of garnet in (a) low-Mg eclogites, (b) high-Mg eclogites with inset showing enlargement of MREE to highlight Eu anomalies and 1σ uncertainties, (c) high-Ca eclogites, (d) pyroxenites and (e) volatile-bearing eclogites. Normalized to chondrite values of McDonough & Sun (1995).

and YK1952 are similar, although at different abundances, with only modest $LREE_N$ over $HREE_N$ enrichment and strong depletions in Zr_N relative to neighbouring elements (Fig. 8d).

Clinopyroxenes in the volatile-rich samples have flat patterns and high abundances from La_N to Sm_N and smooth negative slopes from Sm_N to Lu_N. Niobium, Sr and Ti are noticeably depleted relative to elements of similar compatibility (Fig. 8e).

Trace-element partitioning

To assess whether coexisting phases are in trace-element equilibrium, we calculated apparent cpx–garnet distribution coefficients and compared them with those

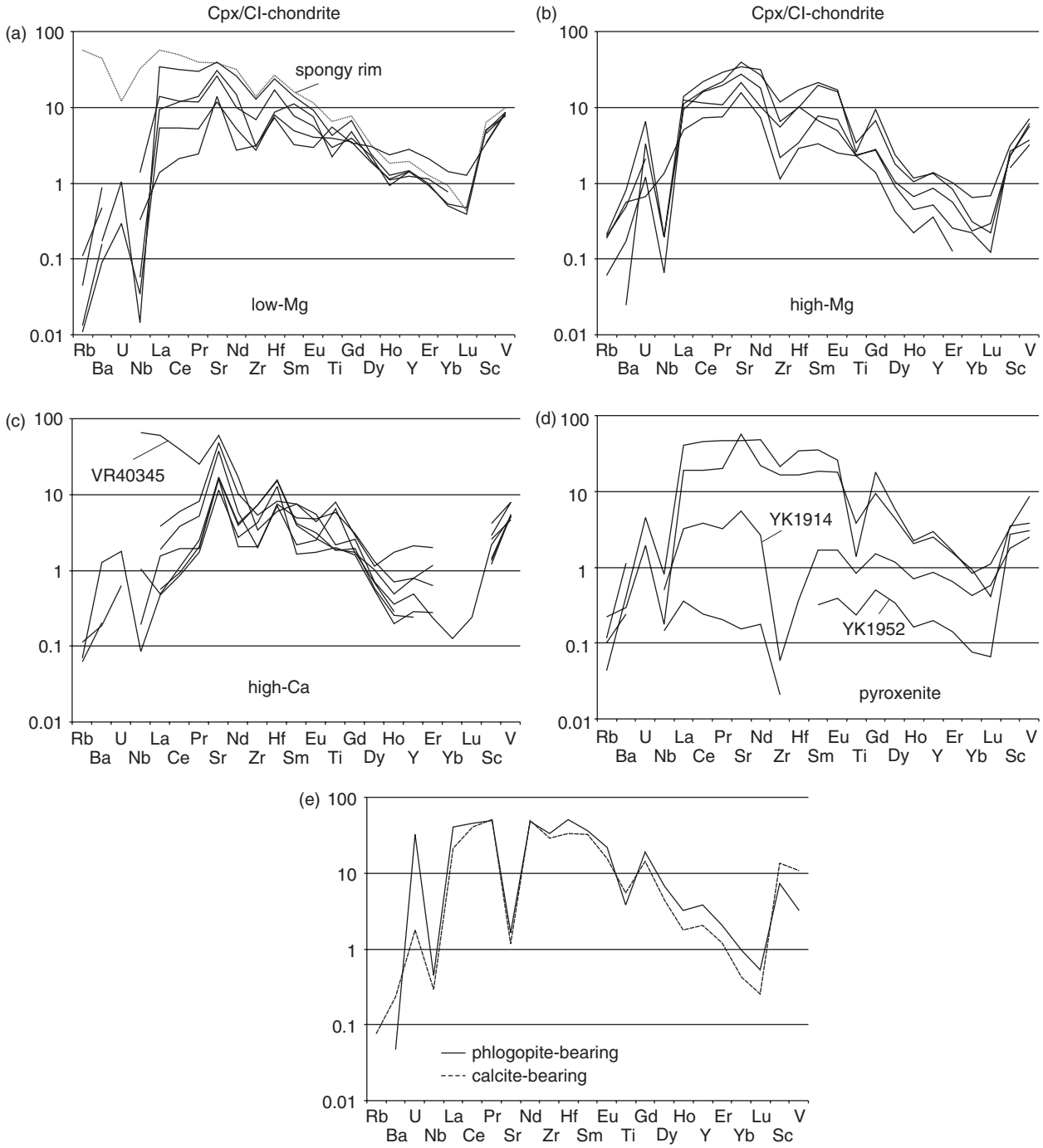

Fig. 8. Extended trace-element patterns of cpx, as in Fig. 7.

determined experimentally or in demonstrably equilibrated natural samples. Low-Mg and high-Mg eclogites have $D^{cpx/garnet}$ for most elements that are within the range determined for natural equilibrated eclogites and experimental assemblages (Harte & Kirkley, 1997; Green *et al.*, 2000; Barth *et al.*, 2002*a*) (Electronic Appendix 7). High-Ca eclogites plot at the low end of the range of distribution coefficients, and have very low D_{MREE} and D_{HREE}, outside the range indicated by the dataset of Harte & Kirkley (1997), who noted that D_{REE} decreases with increasing Ca content in eclogitic minerals. These assemblages are therefore considered to be in equilibrium.

Pyroxenite VR40384 has D values similar to eclogites, but at the high end of the range determined by Harte &

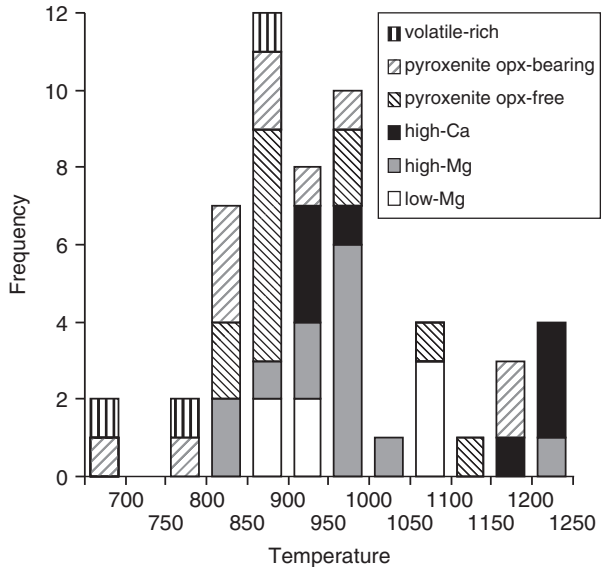

Fig. 9. Histogram of T_{Krogh} (Krogh, 1988) obtained at a preset pressure of 5 GPa, except opx-bearing pyroxenites, where T_{BKN} was solved simultaneously with P_{BKN} (Brey & Köhler, 1990).

Kirkley (1997) (Electronic Appendix 7). Another group (YK1914 and YK1952) plots at the low end, but D_{Hf}, D_{Zr}, D_{Ti} and D_V are far below the values indicated by experimental datasets. Because pyroxenites compositionally grade into eclogites, their drastically different D_{HFSE} values suggest disequilibrium. In contrast, volatile-bearing samples have D_{HFSE} values that appear to be too high to be in equilibrium; however, this may be a consequence of their unusual bulk chemical composition (Ti- and K-rich), which differs substantially from that of 'normal' eclogites and experimental charges.

GEOTHERMOBAROMETRY

Following Schmidberger *et al.* (2007), temperatures of last equilibration were calculated for eclogitic and opx-free pyroxenitic assemblages using the formulation of Krogh (1988). The results are summarized in Table 2 and Electronic Appendix 8 for a preset pressure of 5 GPa and illustrated as a histogram in Fig. 9. For opx-bearing pyroxenites temperatures were calculated simultaneously with pressure [Ca-in-opx thermometry and Al-in-opx barometry, using the formulations of Brey *et al.* (1990)], to constrain their relative positions in the mantle column.

Minerals in some eclogites from Lac de Gras show distinct core and rim compositions or inhomogeneities. Temperatures were not calculated for samples with spatially irresolvable inhomogeneous garnet compositions (SE01, VR43479, VR43480). For eclogites with spongy cpx, core compositions were used in the calculation. Temperatures were calculated for both core and rim compositions, where applicable. For all samples, these temperatures agree within the uncertainty of this thermometer (~50°C; Brey & Köhler, 1990).

Most equilibration temperatures for eclogites lie between 800 and 1000°C (Fig. 9). The transition between the shallow and the deep lithospheric mantle layers in the central Lac de Gras area lies in this temperature interval (Griffin *et al.*, 1999; Pearson *et al.*, 1999). Eclogites in this study lack the distinct bimodal temperature distribution observed by Schmidberger *et al.* (2007), but, as in their study, high-Ca eclogites give higher average temperatures (1080°C; corresponding to a depth of ~155 km if equilibrated along a 40 mW/m^2 geotherm) than other eclogites types (~980°C, depth ~135 km); the diamond-bearing sample (VR40345) gives the highest temperature of the dataset. High Na_2O contents in garnet from high-Ca eclogites are qualitatively consistent with higher equilibration pressures (Sobolev & Lavrent'yev, 1971), as are high K_2O contents in coexisting cpx (Erlank & Kushiro, 1970), suggesting that high-Ca eclogites not only equilibrated at high temperature but also high pressure, rather than representing a temperature excursion. Pyroxenites, both opx-bearing and opx-free, give somewhat lower average temperatures than eclogites (mean ~925°C) and phlogopite-rich eclogites give the lowest temperatures (685 and 769°C, respectively). The calcite-bearing eclogite VR67112b gives a relatively low equilibration temperature of 855°C.

MEASURED AND RECONSTRUCTED WHOLE-ROCKS

Rationale and approach

Kimberlite-borne xenoliths sometimes show evidence for infiltration of the host kimberlite (e.g. Taylor & Neal, 1989; Barth *et al.*, 2001, 2002*b*; Heaman *et al.*, 2006). We therefore follow the standard approach of calculating whole-rock compositions from the compositions of the constituent phases weighted by their modal abundances. Only core compositions were used, as distinct rim compositions may point to late diffusion of elements from kimberlite-related melt veins.

Many eclogitic whole-rock compositions reconstructed with only garnet and cpx have negative Ti anomalies (not shown). For most of these samples rutile or ilmenite has been identified as part of the mineral assemblage and these phases should, therefore, be considered in the whole-rock reconstruction. Rutile or ilmenite modes were estimated by assuming that the bulk-rock has no Ti anomaly when normalized to a normal mid-ocean ridge basalt (N-MORB) composition, and calculating the amount of rutile required to erase the Ti anomaly.

It is of course possible that the eclogites had negative or positive Ti anomalies relative to elements of similar compatibility (Eu and Dy). Because we reconstructed

whole-rock compositions from mineral core compositions, kimberlite infiltration is unlikely to have caused fractionation of Ti from Eu and Dy. In a study in which rutile modes were estimated from the differences between Ti in measured bulk-rocks and in bulk-rocks reconstructed with only garnet and cpx, only three of 19 eclogites reconstructed with rutile show Ti anomalies (Barth *et al.*, 2002*a*). Even eclogite xenoliths with depleted Zr and Hf abundances that resemble those of modern island arc basalts do not show Ti anomalies (Jacob & Foley, 1999). We therefore consider our approach to be a reasonably robust means of obtaining meaningful rutile modes where small sample sizes preclude reliable determination of the modes of accessory phases by point-counting. Where rutile was not recognized on thin-section scale or not analysed, the average eclogitic rutile composition was used for the reconstruction.

Uncertainties

Reconstructing whole-rock compositions in this way is a rather crude method, given the coarse grain size of the eclogites relative to the sample size and the non-uniform distribution of the principal minerals on thin-section scale. The uncertainty in mineral modes of medium- to coarse-grained eclogites with grains >5 mm has been estimated by Jerde *et al.* (1993) to be ~10%, plus uncertainties related to partial alteration, which is minor in our samples. Nevertheless, the whole-rock trace-element budget is rather insensitive to the exact modes for common eclogitic assemblages and REE patterns, which encompass most other elements in terms of compatibility in garnet and cpx, do not change significantly even for modal variations of 30% (Jerde *et al.*, 1993). This is not true for major-element concentrations, which vary substantially with variations in mineral modes, and we therefore do not calculate whole-rock major-element contents.

Because the discussion that follows is based on trace-element patterns and trends rather than absolute abundances, whole-rock reconstruction based on mineral modes is adequate. We are confident that the uncertainty inherent in this approach is not leading to significant misrepresentation of eclogite whole-rock compositions because the trace-element patterns of the reconstructed whole-rocks show distinct differences (see below) that correlate with the assignment to eclogite types based on garnet major-element composition, and this is independent of mineral mode. Following Jerde *et al.* (1993), in Electronic Appendix 9 we show variations in trace-element pattern for one sample in each eclogite type for variations in garnet and cpx abundance from 70:30 to 30:70 vol. %. This shows that the trace-element patterns are generally insensitive to cpx:gt ratios with regard to slopes and anomalies, such as positive Sr, Pb and Eu anomalies, with the exception of the positive Eu anomaly in high-Mg eclogite VR43479, which disappears if a high cpx mode is assumed (not shown). Variations in rutile modes by 50% (Electronic Appendix 9d) lead, as would be expected, to the appearance of Ti anomalies, but a rutile mode of 0·5 instead of 1 vol. % does not erase the positive Nb anomaly in low-Mg eclogite VR50909.

Because of the robustness of the relative trace-element abundances in the reconstructed eclogites, a garnet proportion of 0·65 and cpx proportion of 0·35, approximately the median modal abundances of these minerals in volatile-free eclogites from Lac de Gras, are assumed for eclogite samples that are too small for determination of meaningful modes by point-counting.

Within- and between-group variations

The trace-element compositions of reconstructed whole-rocks are given in Table 4. N-MORB-normalized trace-element patterns of reconstructed whole-rocks are shown in Fig. 10. The three eclogite groups have distinct trace element patterns that are particularly obvious for the REE (Fig. 11). Low-Mg eclogites have positive Pb and Sr anomalies and smooth positive slopes in their $MREE_N$ and $HREE_N$. $LREE_N$ are enriched relative to $MREE_N$ in three samples (Fig. 11a). Three samples have high Nb relative to similarly compatible elements and compared with most other eclogites (Fig. 10a). All high-Mg eclogites display more or less pronounced positive Eu and Sr anomalies and most have positive Pb, and negative Zr and P anomalies. Their N-MORB-normalized REE patterns show shallow positive slopes from La_N to Pr_N or Nd_N and a weak negative slope from Nd_N to Lu_N (Fig. 11b).

VR43479 is a low-Mg eclogite with regard to its garnet Ca–Fe–Mg composition, but has a trace-element pattern typical of high-Mg eclogites and will be discussed with the latter. Conversely, sample YK1949, a high-Mg eclogite in terms of its garnet Ca–Fe–Mg compostion, is more similar to low-Mg eclogites in terms of its whole-rock trace-element pattern and is plotted in Figs 10a and 11a. Whereas the patterns of most samples within the group resemble each other, the N-MORB-normalized incompatible-element abundances of the high-Ca eclogites vary by more than an order of magnitude (Fig. 10c). All samples have positive Pb anomalies and most have positive Sr anomalies. Some samples have negative P and/or Zr anomalies. Niobium abundances in three of the samples are very high, similar to those for some low-Mg eclogites. High-Ca eclogites tend to have flatter $MREE_N$ and $HREE_N$ patterns and more uniform HREE abundances that the other eclogite types, with humps between Sm_N and Ho_N.

The phlogopitized sample YK1911 shows a strong positive Pb anomaly and lower HREE abundances than the calcite-bearing sample VR67112b, which shows a distinct negative Eu anomaly and a depletion of La relative to Ce (Figs 10d and 11d).

Table 4: Trace-element compositions of reconstructed whole-rocks (ppm)

Sample	P	Sc	Ti	V	Co	Ni	Ga	Sr	Y	Zr	Nb	La	Ce	Pr	Nd
Low-Mg eclogites															
vr19674-g4	186	50	4649	317	57	59	14·4	77	24	30	3·6	1·3	3·1	0·5	2·4
vr43452	154	39	2253	328	49	84	17·6	52	32	11	0·1	0·2	0·7	0·1	0·8
vr43469	38	65	4377	349	54	91	14·2	34	28	15	0·2	0·5	1·5	0·3	1·7
yk1926	144	45	3406	258	52	87	14·5	89	18	18	2·0	0·9	2·9	0·6	3·3
yk1943	173	46	5732	295	41	39	14·6	122	25	48	8·2	3·4	8·5	1·3	6·4
yk1949[1]	102	34	1693	158	31	49	10·0	46	10	14	0·3	0·9	2·1	0·3	1·7
High-Mg eclogites															
vr19677-g2	138	39	5160	291	41	53	11·9	98	14	22	0·4	1·3	5·3	1·1	6·4
vr43479[2]	46	25	1265	129	36	126	8·4	56	3	7	0·4	0·6	2·5	0·4	2·3
vr67360	49	36	1573	138	64	184	11·1	76	5	9	0·4	0·9	3·8	0·7	3·3
yk1946	153	28	4877	192	45	105	12·4	108	12	48	0·3	1·0	3·8	0·8	5·0
High-Ca eclogites															
vr19674-g5	267	30	7663	200	41	67	19·5	32	23	43	7·7	0·1	0·4	0·2	1·6
vr40345	0	33	2821	175	47	98	21·0	179	13	13	6·6	6·0	10·9	1·1	3·8
vr43465	142	27	5104	220	31	83	12·1	197	14	35	2·9	0·5	2·2	0·5	4·0
vr50858	295	30	6898	201	44	94	15·0	48	22	38	0·6	0·1	0·3	0·2	2·0
vr50860	68	57	5672	418	57	71	18·6	109	19	11	0·2	0·2	1·3	0·3	2·6
vr50909	238	28	7295	201	42	92	17·1	48	20	57	1·3	0·1	0·4	0·2	2·1
yk3528	91	51	3712	341	53	155	17·7	49	16	9	0·1	0·2	0·8	0·2	1·1
Volatile-rich eclogites															
vr67112b	40	84	9242	521	46	30	10·7	4	40	66	3·1	2·6	12·6	2·4	12·5
yk1911	31	39	9428	286	44	82	16·4	3	23	52	6·4	1·8	5·2	0·9	4·6
Pyroxenites															
yk1914	111	49	707	207	48	547	4·4	31	4	3	0·2	0·6	1·9	0·3	1·0

Sample	Sm	Eu	Eu/Eu*	Gd	Dy	Ho	Er	Yb	Lu	Hf	Pb	Th	La/Lu	K_2O/Th
Low-Mg eclogites														
vr19674-g4	1·1	0·5	1·0	2·2	3·9	1·0	2·9	3·3	0·6	1·2	0·5	0·28	2·4	0·08
vr43452	0·4	0·2	0·8	1·3	3·8	1·2	4·1	4·9	0·8	0·5	0·1	n.d.	0·2	n.a.
vr43469	1·1	0·5	0·9	2·5	4·4	1·1	3·4	3·6	0·6	0·7	0·2	0·01	0·9	1·29
yk1926	1·2	0·5	1·1	1·9	3·0	0·7	2·2	2·4	0·4	0·7	0·3	0·04	2·3	0·90
yk1943	2·1	0·8	1·0	2·9	4·2	1·0	3·0	3·2	0·5	1·6	0·5	0·13	6·5	0·17
yk1949[1]	0·6	0·3	1·1	0·8	1·4	0·4	1·4	1·8	0·3	0·4	0·2	0·03	2·9	1·15
High-Mg eclogites														
vr19677-g2	2·0	0·8	1·2	2·1	2·4	0·5	1·5	1·5	0·3	0·5	0·5	0·07	5·2	68·11
vr43479[2]	0·5	0·2	1·2	0·5	0·6	0·1	0·4	0·3	0·0	0·3	0·1	0·01	9·8	0·37
vr67360	0·6	0·3	1·4	0·6	0·9	0·2	0·6	0·6	0·1	0·2	0·2	0·02	8·6	0·00
yk1946	1·8	0·7	1·2	2·1	2·2	0·5	1·3	1·2	0·2	1·1	0·3	0·06	5·6	1·12
High-Ca eclogites														
vr19674-g5	1·7	0·9	1·1	3·3	4·3	0·9	2·4	2·3	0·4	1·6	0·5	0·07	0·2	0·11
vr40345	0·9	0·4	1·0	1·2	2·2	0·6	1·6	1·4	0·2	0·5	n.d.	n.d.	29·8	n.a.

(continued)

Table 4: Continued

Sample	Sm	Eu	Eu/Eu*	Gd	Dy	Ho	Er	Yb	Lu	Hf	Pb	Th	La/Lu	K_2O/Th
vr43465	2·2	0·9	1·2	2·5	2·6	0·6	1·5	1·4	0·2	1·0	0·4	0·01	2·5	0·40
vr50858	2·0	0·8	0·9	3·3	4·1	0·8	2·2	2·1	0·3	1·0	0·1	n.d.	0·2	n.a.
vr50860	1·4	0·7	1·1	2·7	3·7	0·8	2·2	1·8	0·3	0·6	0·0	n.d.	0·6	n.a.
vr50909	2·0	1·0	1·2	3·3	3·8	0·7	2·0	2·0	0·3	1·6	0·1	0·02	0·2	1·81
yk3528	0·8	0·5	1·1	2·0	3·0	0·7	1·8	1·8	0·2	0·5	0·1	n.d.	0·8	n.a.
Volatile-rich eclogites														
vr67112b	3·8	1·0	0·7	5·3	7·4	1·5	4·1	3·4	0·4	1·8	0·3	0·12	6·0	0·04
yk1911	2·0	0·7	0·8	3·5	3·9	0·7	1·8	1·7	0·2	1·0	1·4	n.d.	7·3	n.a.
Pyroxenites														
yk1914	0·2	0·1	1·1	0·4	0·8	0·2	0·5	0·6	0·1	0·1	0·3	0·03	6·8	1·01

[a]Garnet has Ca–Mg–Fe relationship typical of high-Mg eclogites, but whole-rock trace-element pattern is typical of low-Mg eclogites.
[b]Garnet has Ca–Mg–Fe relationship typical of low-Mg eclogites, but whole-rock trace-element pattern is typical of high-Mg eclogites.

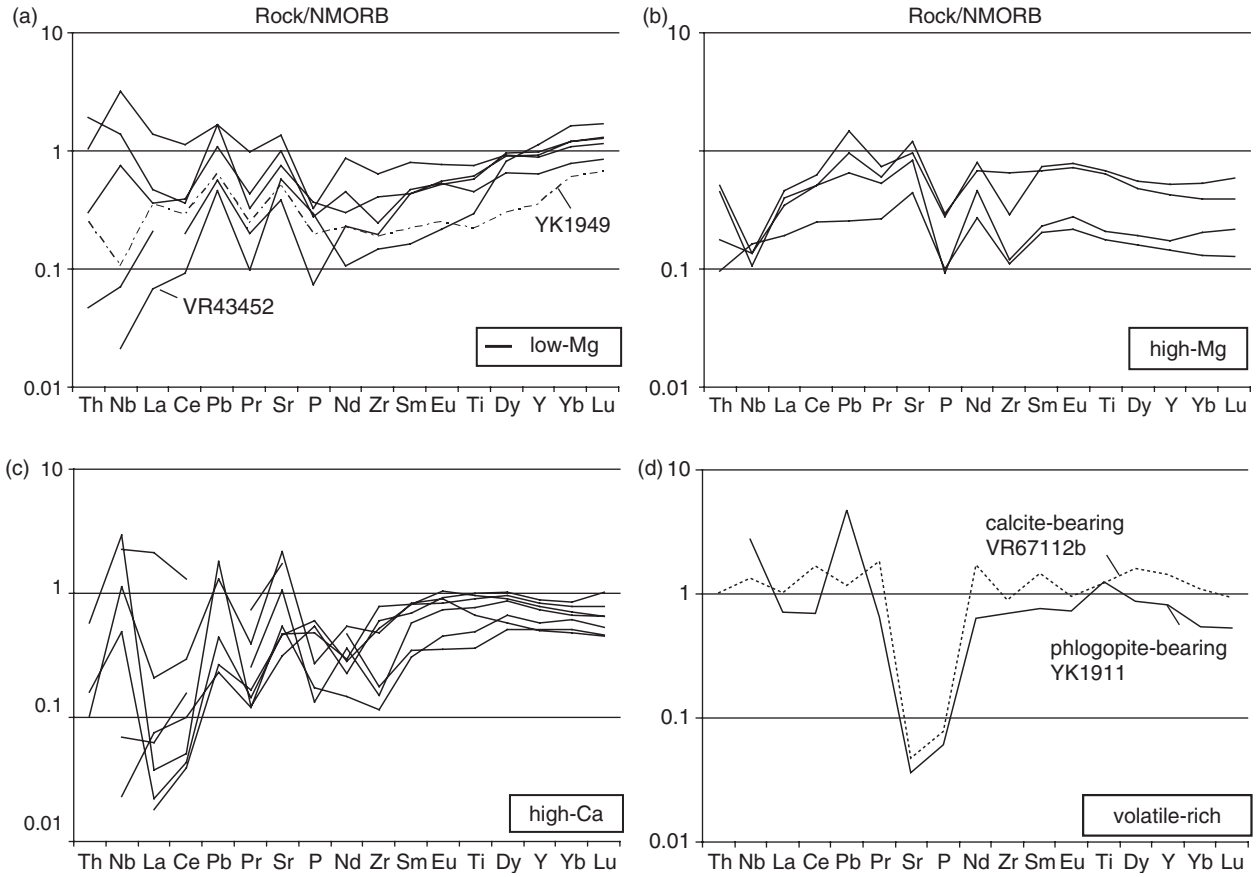

Fig. 10. Extended trace-element patterns of reconstructed (a) low-Mg eclogites, (b) high-Mg eclogites (c) high-Ca eclogites and (d) volatile-bearing eclogites. Normalized to N-MORB of Sun & McDonough (1989).

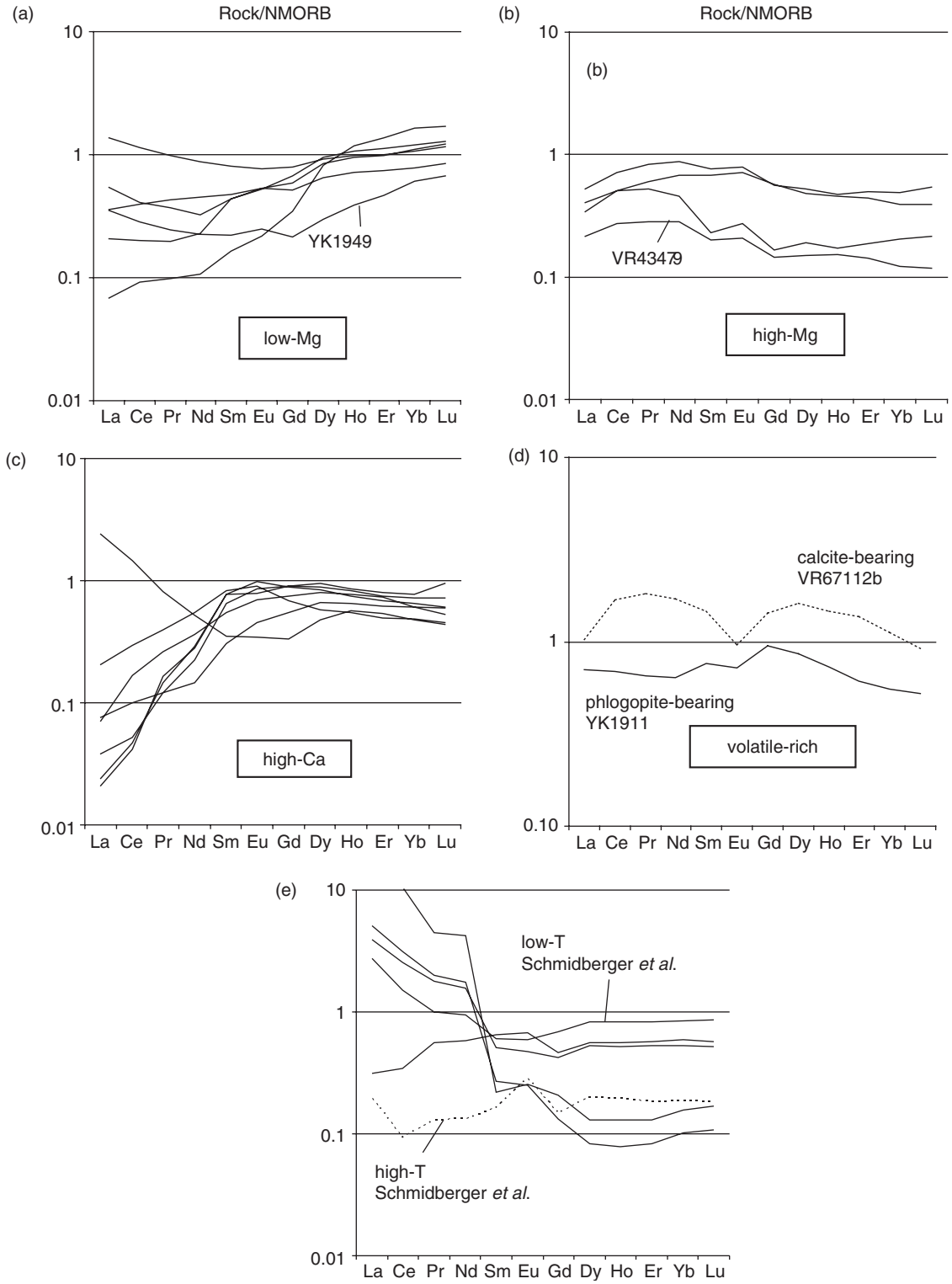

Fig. 11. N-MORB normalized REE patterns for (a) low-Mg eclogites, (b) high-Mg eclogites, (c) high-Ca eclogites and (d) volatile-rich eclogites. Shown for comparison in (e) are reconstructed eclogites from Schmidberger *et al.* (2007).

Both volatile-rich whole rocks display strong negative Sr anomalies. Strontium can be sited in calcite or apatite and/or indicate the presence of a Sr-rich mineral that was not identified in thin section, such as barite.

Four of the six reconstructed whole-rocks in the study of Schmidberger *et al.* (2007) (Fig. 11e) show marked $LREE/HREE_N$ enrichment that is observed only in one high-Ca eclogite in our study (Fig. 11c), suggesting that many of the eclogites they studied were affected by metasomatic LREE enrichment. Two samples in their study that are not affected by this enrichment show positive Eu anomalies similar to the high-Mg eclogites in this study, whereas the distinctive REE pattern of the low-Mg eclogites is not recognized among their samples.

SR–ND–HF ISOTOPE SYSTEMATICS

Strontium, Nd and Hf isotope data for optically pure mineral separates and reconstructed whole-rocks are given in Table 5. Spongy rims and alteration are likely to be mostly removed during leaching in 6N HCl in combination with repeated ultrasonication. Despite this rigorous treatment, the reproducibility of Nd in garnet VR43469 and in cpx YK1914 is worse than for other samples. This may be due to inhomogeneities related to late Nd diffusion, possibly from grain boundaries containing a kimberlite component. The reproducibility of the $^{176}Hf/^{177}Hf$ data is generally poorer than that of Nd, which may reflect a combination of matrix effects caused by imperfectly purified solutions and sample heterogeneity. Parent–daughter ratios are available only from *in situ* analyses, which are not precise enough to allow meaningful model age or initial isotope ratio calculations (i.e. at the time of kimberlite eruption). Because the Lac de Gras kimberlites are relatively young (55–56 Ma; Graham *et al.*, 1999), age correction would result in only a minor change in isotope composition, which is inconsequential in view of the range of compositions displayed by most samples and hence has no effect on the conclusions drawn.

Clinopyroxenes in five volatile-free eclogites and a pyroxenite have Sr isotope ratios ranging from 0·701662 to 0·703546; this range is similar to, or somewhat lower than, that of the depleted mantle at the time of kimberlite emplacement (0·703; Bell & Tilton, 2002). Clinopyroxene in the phlogopitized sample has a distinctly high $^{87}Sr/^{86}Sr$ of 0·751186.

Clinopyroxene controls 56–92% of the Nd budget (Nd concentration in cpx weighted by mode). Neodymium isotope ratios range from 0·511660 to 0·514844. This corresponds to ε_{Nd} variation (per 10 000 deviation of $^{143}Nd/^{144}Nd$ in the sample from $^{143}Nd/^{144}Nd$ in the chondritic mantle model reservoir) from −17 to +43; cpx in the low-Mg eclogites have higher ε_{Nd} than those in high-Mg eclogites. Garnets have generally have higher $^{143}Nd/^{144}Nd$, from 0·512984 ($\varepsilon_{Nd} = +7$) to 0·520965 ($\varepsilon_{Nd} = +162$). Garnets in the two volatile-rich samples have the highest ratios, 0·522790 for garnet in the calcite-bearing sample VR67112b ($\varepsilon_{Nd} = +198$) and 0·525721 in the phlogopitized eclogite YK1911 ($\varepsilon_{Nd} = +255$).

Garnet contributes 18–32% and cpx 48–78% of the Hf budget. The proportion controlled by rutile is 4–30% (Aulbach *et al.*, in preparation). Measured $^{176}Hf/^{177}Hf$ in cpx ranges from 0·281263 in phlogopite-bearing sample YK1911 ($\varepsilon_{Hf} = -53$) to 0·286130 in low-Mg eclogite VR43469 ($\varepsilon_{Hf} = +119$), and in garnet from 0·283958 in pyroxenite YK1915 ($\varepsilon_{Hf} = +42$) to 0·295718 in low-Mg eclogite YK1926 ($\varepsilon_{Hf} = +458$). Hafnium in garnet in the phlogopite–apatite-bearing sample is extremely radiogenic ($^{176}Hf/^{177}Hf = 0·354367$), corresponding to an ε_{Hf} of +2532, which is close to a value determined for a garnet separate from a Roberts Victor eclogite ($\varepsilon_{Hf} = +256$l; Jacob *et al.*, 2005). Garnet in the calcite-bearing sample has extremely radiogenic Nd and Hf ($\varepsilon_{Nd} = +193$, $\varepsilon_{Hf} = +2516$). Garnet in pyroxenite YK1915 also has radiogenic Nd and Hf ($\varepsilon_{Nd} = +27$, $\varepsilon_{Hf} = +42$).

Despite the large uncertainties for reconstructed whole-rocks (calculated as the square root of the sum of squared uncertainties of two standard errors for garnet and cpx analyses, combined with 20% propagated uncertainty on the proportion of Nd or Hf, respectively, contributed by each mineral), the isotopic data are consistent in that they correlate with the independently determined parent–daughter ratios: (1) Low-Mg eclogites have higher Sm/Nd reflected in the steeper positive slope of their N-MORB-normalized REE patterns (Fig. 11a) compared with the high-Mg eclogites (Fig. 11b). Accordingly, reconstructed low-Mg eclogites have higher present-day ε_{Nd} (0 to +47) than high-Mg eclogites (−4 and −17). (2) Low-Mg eclogite YK1943 has very high Nb and LREE abundances that could have been added during metasomatism that also enhanced its Hf abundance. This sample has the lowest ε_{Nd} and ε_{Hf} of the low-Mg eclogites (0 and +20, respectively). In contrast, apparently unenriched low-Mg eclogites have more radiogenic Nd and Hf ($\varepsilon_{Nd} = +47$ and +9; $\varepsilon_{Hf} = +128$ and +113, respectively).

The Sr–Nd isotope diagram reveals that ε_{Nd} in cpx varies from −19 to 43 at nearly constant, depleted-mantle-like $^{87}Sr/^{86}Sr$ (Fig. 12a). In the Nd–Hf isotope diagram (Fig. 12b), the reconstructed whole-rocks lie on curved mixing lines if the 'mixing' proportions of Nd and Hf for the two 'end-member' minerals are very different (e.g. YK1911). Garnets have more radiogenic Nd and Hf than coexisting cpx. All reconstructed volatile-free eclogites plot in the radiogenic field with regard to Hf or are isotopically similar to the depleted mantle. Two high-Mg eclogites and one low-Mg eclogite have unradiogenic Nd, one high-Mg eclogite has radiogenic Nd, and

Table 5: Individual and averaged Sr, Nd and Hf isotope ratios obtained from garnet and cpx solutions

Sample	$^{87}Sr/^{86}Sr$	2SE/2SD	$^{143}Nd/^{144}Nd$	2SE/2SD	ε_{Nd}	2SE/2SD	$^{176}Hf/^{177}Hf$	2SE/2SD	ε_{Hf}	2SE/2SD
Low-Mg eclogites										
VR43469 cp	0·702661	0·000010	0·514844	0·000006	43	0·1	0·286130	0·000012	119	0·4
VR43469 gt			0·515508	0·000014	56	0·3	0·286506	0·000012	132	0·4
VR43469 gt r			0·515453	0·000010	55	0·2	0·286548	0·000011	134	0·4
VR43469 gt r			0·515384	0·000007	54	0·1	0·287244	0·000010	158	0·4
VR43469 gt r			0·515487	0·000014	56	0·3	0·286996	0·000014	149	0·5
VR43469avg gt			0·515458	0·000109	55	2·1	0·286823	0·000715	143	25·3
WR VR43469			*0·515059*	*0·000273*	*47*	*5*	*0·286405*	*0·001079*	*128*	*38*
YK1926 cp	0·703546	0·000011	0·513043	0·000007	8	0	0·283154	0·000009	13	0·3
YK1926 gt			0·513364	0·000008	14	0·1	0·295718	0·000005	458	0·2
WR YK1926			*0·513120*	*0·000026*	*9*	*1*	*0·285980*	*0·000716*	*113*	*25*
YK1943 cp			0·512143	0·000007	−10	0·1	0·282213	0·000005	−20	0·2
YK1943 gt			0·514461	0·000012	36	0·2	0·287510	0·000008	168	0·3
YK1943 gt r			0·514491	0·000009	36	0·2	0·287332	0·000005	161	0·2
YK1943 gt r			0·514517	0·000010	37	0·2	0·287290	0·000007	160	0·2
YK1943avg gt			0·514489	0·000056	36	1·1	0·287377	0·000233	163	8·2
WR YK1943			*0·512625*	*0·000228*	*0*	*5*	*0·283138*	*0·000879*	*13*	*31*
High-Mg eclogites										
VR43480 gt			0·520965	0·000017	162	0·3	0·284950	0·000010	77	0·4
VR67360 cp							0·283509	0·000074	26	2·6
VR67360 cp r							0·283433	0·000031	23	1·1
VR67360avg cp	0·701662	0·000018	0·511660	0·000010	−19	0·2	0·283471	0·000108	25	3·8
VR67360 gt			0·512984	0·000101	7	2·0	0·287429	0·000180	165	6·4
WR VR67360			*0·511761*	*0·000132*	*−17*	*3*	*0·284734*	*0·000469*	*69*	*17*
YK1949 cp	0·703019	0·000013	0·512231	0·000009	−8	0·2	0·282513	0·000009	−9	0·3
YK1949 gt			0·513511	0·000010	17	0·2	0·290297	0·000042	266	1·5
YK1949 gt r			0·513508	0·000012	17	0·2	0·289947	0·000015	254	0·5
YK1949 gt r			0·513552	0·000014	18	0·3				
YK1949avg gt			0·513523	0·000049	17	1·0	0·291569	0·000494	311	17·5
WR YK1949			*0·512446*	*0·000103*	*−4*	*2*	*0·284622*	*0·000847*	*65*	*30*
Volatile-rich eclogites										
VR67112b gt			0·522790	0·000008	198	0·2	0·354367	0·000036	2532	1·3
YK1911 cp	0·751186	0·000009	0·512165	0·000007	−9	0·1	0·281263	0·000009	−53	0·3
YK1911 gt			0·525721	0·000013	255	0·3	0·288051	0·000012	187	0·4
WR YK1911			*0·513940*	*0·000342*	*25*	*7*	*0·281414*	*0·000018*	*−48*	*1*
Pyroxenites										
YK1914 cp	0·703015	0·000034	0·513283	0·000041	13	0·8				
YK1914 cp r	0·702956	0·000005	0·513200	0·000027	11	0·5				
YK1914 cp r			0·513527	0·000059	17	1·1				
YK1914 cp r			0·513045	0·000010	8	0·2				
YK1914avg cp	0·702986	0·000083	0·513264	0·000402	12	7·8				
YK1915 gt			0·514003	0·000011	27	0·2	0·283958	0·000021	42	

Analyses of full procedural replicates are designated with an 'r' after sample name. SE, standard error (internal error, single analyses); SD, standard deviation (external error, averaged multiple analyses). Italics used for reconstructed whole-rocks (mineral isotopic compositions and concentrations weighted by modes). Uncertainties for reconstructed whole-rocks include 2SE or 2SD uncertainties on each mineral's isotope composition combined with 20% uncertainty in the amount of Nd or Hf contributed by the constituent minerals. ε_{Nd} and ε_{Hf} are per 10 000 deviation from model chondritic mantle [model of Wasserburg *et al*. (1981) and Blichert-Toft & Albarède (1997), respectively].

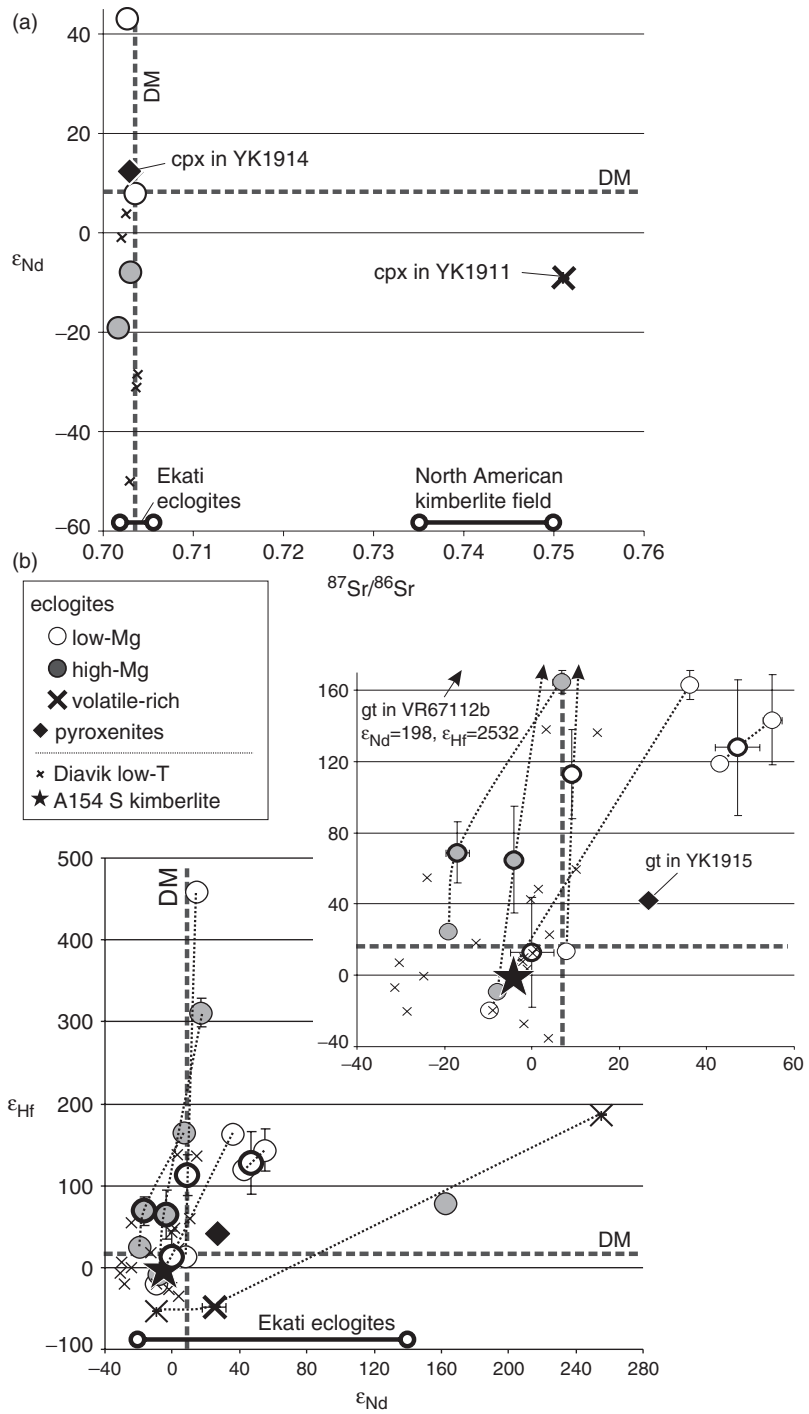

Fig. 12. (a) Sr–Nd for cpx and (b) Nd-Hf isotope diagram for garnet, cpx and reconstructed whole-rocks (symbols with bold outline). Fine dashed lines in (b) connect data points from the same sample, with garnets having more radiogenic isotopic compositions. Uncertainties for reconstructed whole-rocks combine 20% modal uncertainty with uncertainties on each mineral's isotope composition. Error bars on individual minerals may be smaller than the symbols. Also shown are the isotopic compositions of the depleted mantle (DM; DePaolo, 1981; Griffin *et al.*, 2000; Bell & Tilton, 2002). Range of $^{87}Sr/^{86}Sr$ in eclogites from Ekati (Lac de Gras area, ~100 km north of Diavik; Jacob *et al.*, 2003), in North American kimberlites and compositions of low-temperature eclogites from Diavik and of Lac de Gras A154 South kimberlite from Schmidberger *et al.* (2007).

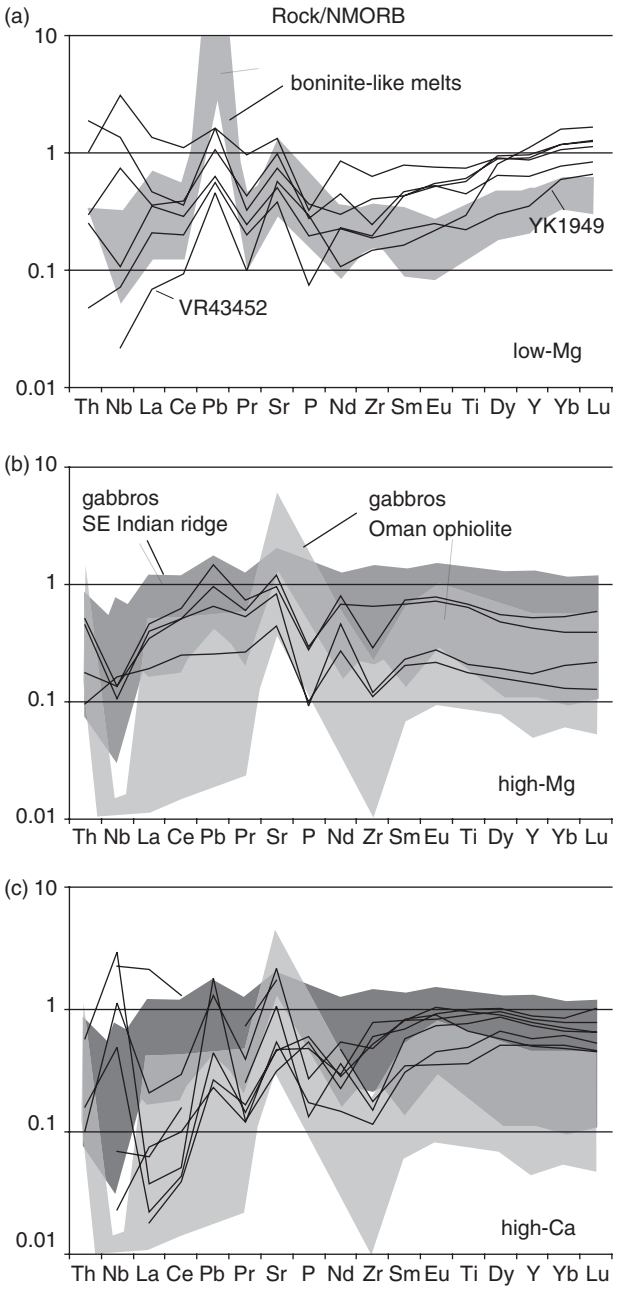

Fig. 13. Trace-element patterns of (a) low-Mg, (b) high-Mg and (c) high-Ca eclogites compared with boninite-like volcanic rocks from the Isua greenstone belt (Polat *et al.*, 2002), gabbros from the Oman ophiolite (Benoit *et al.*, 1996) and the SE Indian Ridge (Hart *et al.*, 1999); normalized to N-MORB of Sun & McDonough (1989).

one low-Mg eclogite has ε_{Nd} similar to the depleted mantle (Fig. 12b).

Clinopyroxene in the phlogopitized eclogite YK1911 has unradiogenic Nd and Hf and strongly radiogenic Sr, whereas the coexisting garnet has radiogenic Nd and Hf. Although this sample contains ~50 vol. % phlogopite, its whole-rock isotopic composition was calculated from garnet and cpx alone because the contribution from phlogopite to the Hf and Nd budget is $<2\%$ and $<1\%$, respectively (unpublished data). The whole-rock has radiogenic Nd but has lower ε_{Hf} than any other sample analysed, in accord with the extreme Hf abundance (5·3 ppm) and low Lu/Hf of the cpx.

DISCUSSION

Origins of eclogites beneath the Slave Craton

High-Mg and high-Ca eclogites

With regard to their major- and trace-element contents, the high-Mg and high-Ca eclogites from Lac de Gras are broadly similar to variably evolved oceanic gabbros (Fig. 13b and c), which may indicate an origin as subducted oceanic crust. Compatible trace-element abundances are useful to deduce potential crustal protoliths, as these elements are less susceptible to post-formation modification (Jacob, 2004). The flat HREE patterns in the high-Mg and high-Ca eclogites are compatible with a low-pressure origin as the oceanic crust is a product of moderate degrees of partial melting mainly within the spinel stability field (e.g. Presnall *et al.*, 2002), whereas melting with residual garnet would qualitatively be expected to produce strongly fractionated REE patterns. Positive Sr and Pb anomalies, although compatible with a plagioclase signature, could also be due to cryptic metasomatism (Dawson, 1984) of the eclogites during their residence in the lithospheric mantle. These anomalies are probably not related to kimberlite infiltration, as the whole-rock eclogite compositions were reconstructed from analyses of fresh mineral cores.

Low Zr/Sm, similar to that in primitive gabbros, is observed for many of the high-Mg and high-Ca eclogites (Fig. 13b and c) and is independent of the ratio of garnet/cpx and whether or not the whole-rock was reconstructed with rutile (Electronic Appendix 10). The negative trend of Mg-number against Yb in garnet (Fig. 14) argues against igneous processes involving garnet accumulation (Taylor & Neal, 1989), as suggested, for example, for some high-Mg eclogites from West Africa (Barth *et al.*, 2002b). Rather, the anti-correlation suggests that olivine fractionation played a role in the formation of the protoliths. Fractionating olivine would exclude Yb ($D^{olivine/basalt} = 0{\cdot}02$; Nikogosian & Sobolev, 1997), and incorporate Mg relative to Fe ($D = 1{\cdot}5$ and $0{\cdot}5$, respectively; Taura *et al.*, 1998), leading to progressive depletion of Mg and enrichment of Yb in the residual melt and hence anti-correlated Mg and Yb in the whole-rock. This is inherited after eclogitization. All eclogite types (except VR43452) plot along the olivine fractionation trend, suggesting that they formed by a similar process.

High-Mg eclogites have lower $\sum$REE than high-Ca eclogites and some appear to have positive Eu anomalies

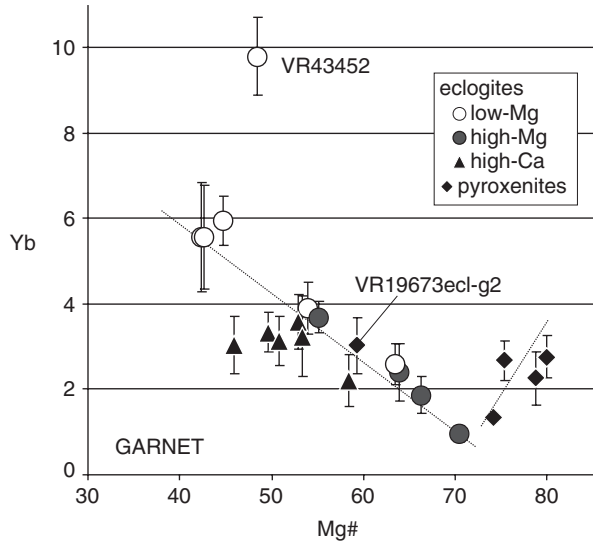

Fig. 14. Garnet Mg-number vs Yb (ppm, including 2σ uncertainty). Lines qualitatively show separate correlations for eclogites (except outlier VR43452) and pyroxenites (except outlier VR19673ecl-g2).

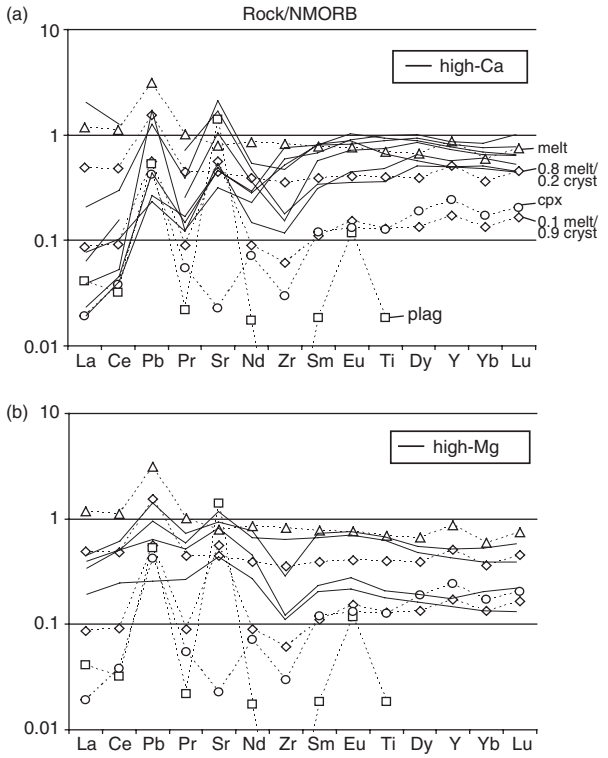

Fig. 15. Reconstructed (a) high-Ca and (b) high-Mg eclogites compared with compositions of plagioclase and cpx crystallizing from a MORB melt modelled using distribution coefficients of Norman *et al.* (2005). The MORB was calculated as a 10% equilibrium melt of MORB pyrolite [composition from Kelemen *et al.* (1993), except Pb, Pr, Sr, Y and Lu, which were calculated as residues from 1% fractional melting of pyrolite from McDonough & Sun (1995) using melt modes of Kinzler (1997) and distribution coefficients of Norman *et al.* (2005)]. Also shown are mixtures of crystals (consisting of 50% plagioclase plus 50% cpx) and melt in the proportions 0·9:0·1 and 0·2:0·8.

(Eu/Eu* up to 1·4), similar to more primitive cumulates (troctolite gabbros and olivine gabbros) reported in the literature (Fig. 13b). Although the sizes of these Eu anomalies are not outside the analytical uncertainty, their correlation with Ce/Yb in reconstructed eclogites supports their significance ($r^2 = 0{\cdot}66$, $n = 4$). The more primitive nature of high-Mg eclogites is consistent with higher Mg-numbers relative to high-Ca eclogites and may be due to olivine accumulation during formation of their protoliths. The two samples with the lowest HREE abundances have the highest Eu/Eu*, which is compatible with variations in plagioclase modes.

More evolved protoliths with higher pyroxene/plagioclase plus trapped melt could account for small or absent positive Eu anomalies and higher ∑HREE of high-Ca eclogites (Fig. 13c). Although the reason for the frequent association of graphite or diamond with high-Ca eclogites is unclear (Aulbach *et al.*, 2003), the frequent occurrence of kyanite in high-Ca eclogites, also observed at Ekati, just north of Lac de Gras, has been argued to support a crustal protolith (Jacob, 2004). Kyanite and/or corundum have been suggested to exsolve from high-temperature, high-Al clinopyroxenes (Caporuscio & Smyth, 1990). Eclogites from Lac de Gras show no exsolution textures suggestive of such an origin, although recrystallization can obscure or destroy microstructural evidence for exsolution (e.g. Griffin *et al.*, 1984).

Modelling shows that, qualitatively, plagioclase accumulation from a low-pressure melt derived from MORB mantle can account for positive Pb, Sr and Eu and negative Zr anomalies relative to N-MORB, whereas cpx accumulation or trapped melt increases Zr, Y, MREE and HREE abundances (Fig. 15). Some melt addition (for example, by entrapment) seems to be required to increase all trace-element abundances to those observed for the eclogites. Although high-Ca and high-Mg eclogites could represent shallow and deep portions of the same oceanic crust, the higher average temperatures obtained for the high-Ca eclogites, the frequent occurrence of carbon in high-Ca eclogites and its absence in high-Mg eclogites, the strong LREE/HREE fractionation observed for six of seven high-Ca eclogites, and the narrow range of compositions of the high-Mg eclogites suggest that they may have protoliths that are not cogenetic. Some discrepancies, in particular affecting the incompatible elements, may be due to post-crystallization processes acting upon the protoliths, such as dehydration, melting and later metasomatism that is evident in peridotites from the same locality (Griffin *et al.*, 1999).

Low K_2O/Th for high-Ca and high-Mg eclogites (average 0·8; Table 4) relative to assumed crustal

precursors (e.g. gabbros, SE Indian Ridge: average 2·2; Hart *et al.*, 1999) may reflect the preferred loss of fluid-mobile elements during dehydration (Becker *et al.*, 2000), although large uncertainties on these low-abundance elements in the constituent minerals and reconstructed whole-rocks makes this interpretation less than robust. The REE patterns of most high-Mg eclogites are too flat to represent melting residues, as partial melting should produce low LREE/HREE (Electronic Appendix 10). In contrast, the marked LREE depletion of five of seven high-Ca eclogites (La/Lu = 0·2–0·8) contrasts with that of assumed evolved gabbroic protoliths (La/Lu = 1·5–32; Hart *et al.*, 1999) and can be modelled as a consequence of partial melting during subduction after eclogitization (i.e. in the presence of garnet, which retains HREE relative to LREE, e.g. Barth *et al.*, 2002*a*) has taken place (Aulbach *et al.*, 2003).

Our results are compatible with previous studies on eclogite xenoliths from the Slave Craton, including those from the same kimberlite, that have linked these samples or some of these samples to Paleoproterozoic subduction events (the 1·95–1·91 Ga formation of the Hottah terrane and the ~1·8 Ga formation of the Great Bear magmatic arc) in the Slave craton (Griffin *et al.* 1999; Kopylova *et al.*, 1999; Heaman *et al.*, 2002, 2006; Schmidberger *et al.*, 2005, 2007).

The compositional features discussed above, although compatible with crustal protoliths, are not necessarily definitive of a subduction origin. However, if direct crystallization from basaltic melts at high pressure (i.e. mantle depths) is invoked instead, specific conditions would have to be met to satisfy the observations. The Mg-number in eclogites from Lac de Gras are lower than those expected of primary high-pressure mantle melts (e.g. Walter, 1998; O'Hara & Herzberg, 2002), requiring crystallization at high pressures after olivine fractionation. This origin would further require shielding from peridotitic wallrock, with which the fractionated melts would no longer be in equilibrium (Barth *et al.*, 2001). In such a setting, the low relative abundances of fluid-mobile elements compared with those of less fluid-mobile elements and of LREE relative to HREE (Table 4) would reflect an expulsion of fluids during crystallization of the protoliths and later melt mobilization, respectively. The eclogites clearly do not represent garnet plus cpx cumulates, which would require a positive correlation of Mg-number with Yb that is at variance with the observed negative correlation in eclogitic garnets from this study (Fig. 14).

Low-Mg eclogites

Garnets in low-Mg eclogites compositionally overlap with those in massive eclogites from Jericho (NW of the Lac de Gras kimberlites) that were suggested to have a high-pressure intrusive origin, based on the similarity of their major-element compositions to those of Group A eclogites from southern Africa, for which a mantle origin has been proposed (Kopylova *et al.*, 1999). Garnets in low-Mg eclogites in the present study have major-element compositions more similar to garnets in group B rather than group A eclogites.

The positive slope in N-MORB-normalized HREE abundances displayed by the low-Mg eclogites is clearly distinct from other eclogite types and is similar to those of boninite-like second-stage melts that are closely associated with ultramafic volcanics (Smithies *et al.*, 2004) (Fig. 13a). The range of Mg-numbers in the low-Mg eclogites (55–66) overlaps with that of Archaean second-stage melts from Isua (58–75) and Abitibi (52–82; Smithies *et al.*, 2004). These similarities might indicate that the low-Mg eclogites have an origin in a previously depleted mantle source, such as supra-subduction zone mantle. Subchondritic Zr/Hf of the low-Mg eclogites contrasts with the supra-chondritic Zr/Hf of the high-Mg and high-Ca eclogites (Aulbach *et al.*, in preparation) and is consistent with previous cpx-controlled depletion in an arc mantle source. This source could have been subsequently remelted to generate the boninite-like precursor to the low-Mg eclogites, as suggested for the protoliths of eclogites from Udachnaya (Jacob & Foley, 1999).

Although some second-stage melts, to which the low-Mg eclogites are similar, are closely associated with komatiites and could contain a plume component, the radiogenic or depleted mantle-like Nd and Hf, and unradiogenic Sr in the low-Mg eclogites do not support plume involvement.

Trace-element and Sr–Nd–Hf isotope constraints on post-formation metasomatism

Several low-Mg and high-Ca eclogites show negative slopes in the LREE, which may be indicative of interaction with small amounts of LREE-enriched melt (Navon & Stolper, 1987), amounting to cryptic metasomatism (i.e. not accompanied by crystallization of new phases) in the nomenclature of Dawson (1984). High Nb abundances relative to elements of similar compatibility displayed by some low-Mg and high-Ca eclogites (Fig. 10) could result from overestimation of rutile modes. However, high-Ca eclogite VR40345 is rutile-free and has been reconstructed without rutile; its high Nb abundance is accompanied by LREE enrichment, indicating that metasomatic addition may be responsible.

Low-Mg eclogites show a positive correlation of La with Nb (Electronic Appendix 11a), indicating concomitant addition of LREE and Nb. This suggests that the metasomatic agent was a solute-rich fluid or silicate silicic melt, as hydrous fluids and carbonatites do not carry enough HFSE to affect the budget of eclogites (Green & Wallace, 1988; Klemme *et al.*, 1995; Adam *et al.*, 1997; Stalder *et al.*, 1998). Of the samples that are enriched in Nb, all but one (high-Ca eclogite VR50909) show a simultaneous enrichment in

Hf (Electronic Appendix 11b). Together, these trace-element relationships suggest that both Sm/Nd and Lu/Hf were lowered in these samples. Their low parent–daughter ratios contrast with higher ratios in unenriched samples and resulted in the ingrowth of a range of Nd and Hf isotope compositions. Compared with the low-Mg and high-Ca eclogites, the high-Mg eclogites have a narrow range of La and Nb concentrations, which correlates with a narrow range in Nd and Hf isotope compositions (Fig. 12).

Precise model ages cannot be calculated because parent–daughter ratios are available only from *in situ* analyses, which have relatively large uncertainties. However, evidence for long-term enrichment and depletion may be discerned. Low-Mg eclogites, even those that are enriched in LREE, have relatively high Sm/Nd as a result of having overall positive slopes in their REE patterns relative to MORB, whereas the high-Mg eclogites have relatively flat REE patterns and therefore lower Sm/Nd (Fig. 11). This translates into lower ε_{Nd} for high-Mg eclogites than for low-Mg eclogites. In contrast, they show no systematic difference with respect to $^{176}Hf/^{177}Hf$. Because the low- and high-Mg eclogites are proposed to have different origins, as discussed above, and therefore did not necessarily have the same initial isotopic composition and formation age, these isotopic differences cannot be used to estimate their ages.

A long-term coupling of trace-element and isotopic abundances is also indicated by the fact that low-Mg eclogite YK1943, which has experienced Nb and LREE addition, has lower ε_{Nd} (0) and ε_{Hf} (+13) than low-Mg eclogite VR43469 with higher Lu/Hf and Sm/Nd ($\varepsilon_{Nd} = +47$; $\varepsilon_{Hf} = +128$). If low-Mg eclogites YK1943 and VR43469 originally had identical initial Nd and Hf isotope compositions and if the parent–daughter ratios are accurate and were modified only once during their evolution shortly after metamorphism (when their isotopic composition would have been reset), this overprint can be calculated for both isotopic systems to have occurred at ~1·7 Ga. This would suggest that Hf and Nd were added during the same event. In contrast, high-Mg eclogites VR67360 and YK1949 would have had identical Nd isotope compositions at ~1·0 Ga, whereas their Hf isotope compositions are disturbed in that the sample with the higher parent–daughter ratio has a lower $^{176}Hf/^{177}Hf$ than the sample with the lower parent–daughter ratio. These results suggest that the LREE and HFSE enrichment observed in different samples occurred during separate events that did not affect the eclogites equally.

Extreme HFSE enrichment leading to the growth of zircon and rutile, and LREE addition leading to the growth of apatite in eclogites from the Jericho kimberlite in the northern Slave craton have been ascribed to two separate metasomatic events at around 1·8 Ga (quasi-coincident with the age of formation and metamorphism) and 1·3–1·0 Ga, respectively (Heaman *et al.*, 2002, 2006; Schmidberger *et al.*, 2005). The authors associated these events with Paleoproterozoic subduction and a Mesoproterozoic thermal disturbance in the Slave lithospheric mantle, possibly linked to the Mackenzie igneous event. Mesoproterozoic Nd model ages mostly between 1·3 and 1·4 Ga were reported for eclogites from the nearby Ekati kimberlites (Jacob *et al.*, 2003). Although we do not observe zircon or apatite in volatile-free eclogites from Lac de Gras and the age constraints obtained from our data are weak, they support a link between these events described for other eclogite populations and the metasomatic enrichment observed in our study.

The Sr isotope data in the present study are similar to those of Schmidberger *et al.* (2007), who suggested that the depleted-mantle-like values are consistent with derivation of the protoliths from an oceanic mantle source. However, $^{87}Sr/^{86}Sr$ in volatile-free eclogites in the present study is remarkably constant considering their Nd and Hf isotope variability (Fig. 12) and the variability of trace-element patterns (Fig. 10). Given the evidence for dehydration and melting in many of the eclogites, fractionation of highly incompatible Rb from Sr and differential ingrowth of radiogenic Sr would be expected. This may indicate a relatively recent overprint and, considering the similarity of $^{87}Sr/^{86}Sr$ to present-day depleted mantle, which is significantly lower than $^{87}Sr/^{86}Sr$ of North American kimberlites, a juvenile (asthenospheric) source.

Pyroxenites

Pyroxenites from Lac de Gras often show relationships in their major-element contents that are different from those observed in the eclogites. For example, pyroxenitic garnets show a negative correlation between CaO and Na_2O contents, whereas these oxides are positively correlated for garnets in eclogites (Fig. 5). CaO is well correlated with Cr_2O_3 in pyroxenitic garnets, but not in eclogitic garnets (Fig. 4). Mg-number is positively correlated with Yb abundance for pyroxenitic garnets, but anti-correlated for eclogitic garnets (Fig. 14). This suggests that the pyroxenites in the present study are not related to the eclogites by fractionation or accumulation processes, as proposed for the origin of some pyroxenites (Foley *et al.*, 2003).

Pyroxenites have also been interpreted as the products of crystal segregation in magma channels, with altered oceanic crust as the magma source; this would explain their Eu anomalies and stable and radiogenic isotope compositions (Pearson *et al.*, 1993; Becker, 1996). As the high-pressure liquidus phases of most terrestrial basalts are cpx and garnet (O'Hara & Herzberg, 2002), partial melts of eclogites with basaltic composition would crystallize cpx and garnet, but not opx. More than half of the pyroxenites from Lac de Gras contain opx, suggesting that they probably did not crystallize directly from eclogite-derived melts.

Low-Cr websterites and pyroxenites could be crystallization products of mafic melts that interacted with peridotitic mantle, thus becoming more refractory. The positive correlation of Yb and Mg-number in garnet would allow an origin by fractional crystallization from such melts. Alternatively, they formed by reaction of silicic (possibly eclogite-derived) melts with mantle peridotites (e.g. Kelemen *et al.*, 1993; Aulbach *et al.*, 2002). This agrees with the similarity of hypothetical melts in equilibrium with pyroxenitic garnets in most samples to eclogite-derived melts (Electronic Appendix 12). Niobium concentrations in all hypothetical melts are much higher than in eclogite-derived melts, regardless of whether or not rutile is assumed to be in the residue. The same is true for La, Ce and Zr concentrations in some samples, which may indicate that Nb ± Zr and LREE were added to the pyroxenites some time after their formation, as discussed in the previous section for some eclogites. Because minimum ages for pyroxenitic rutile with an unradiogenic Hf isotope composition (calculated by projecting the $^{176}Hf/^{177}Hf$ to the model depleted mantle isotopic evolution curve assuming zero ingrowth) range to 1·78 ± 0·66 Ga (Aulbach *et al.*, in preparation), it appears likely that the pyroxenites were not formed recently (e.g. during kimberlite-related or precursory melt migration), and that some of the samples are at least Mesoproterozoic.

Garnet pyroxenite YK1952 consists of schlieren of equilibrated garnet pyroxenite in a 'matrix' of spongy cpx, fine cpx–opx intergrowths, embayed garnet and melt patches (Fig. 2f). Garnet in the pyroxenite schlieren has very low LREE and HFSE abundances. Orthopyroxene in the matrix has distinctly higher Mg-number and Cr-number, and contains more CaO than opx from the pyroxenite schlieren, whereas opx rims in the schlieren are compositionally similar to opx in the matrix. The considerable compositional and textural disequilibrium in this sample suggests that this is a young feature caused by reaction with fluids shortly before or at the time of entrainment.

As a consequence of the small sample sizes of most of the pyroxenites studied here, a comprehensive isotopic dataset is not available. Clearly, more such data are needed, in addition to stable isotope data, to obtain better constraints on the origins of this rock type. Considering the microstructural and compositional variability of the pyroxenites and major-element relationships opposite to those observed for eclogites, it appears certain that pyroxenites form by a variety of processes, some of which are unrelated to the formation of eclogites and their protoliths.

Volatile-rich eclogites

Volatile-rich eclogites from Lac de Gras display the most extreme Hf–Nd isotope systematics of all the analysed samples. Garnets in phlogopitized (YK1911) and in calcite-bearing eclogite (VR67112b) have the most radiogenic Nd (ε_{Nd} = 248·6 and 192·7, respectively). Garnet in VR67112b has extremely high ε_{Hf} (2516). Clinopyroxene in YK1911 has the lowest ε_{Hf} measured for any mineral separate from Lac de Gras (−53), in accord with the very high Hf abundance in its cpx (5 ppm). In contrast, garnet in this sample has radiogenic Hf (ε_{Hf} = 136). This discrepancy is at least in part due to their relatively low equilibration temperatures (769°C and 855°C, respectively), which allowed the isotopic compositions of cpx and garnet to evolve separately at their low and high parent–daughter element ratios, respectively, for extended periods of time and possibly since formation. Accordingly, the cpx in YK1911 gives a minimum Hf age of ~2·7 Ga.

Slab-derived fluids could have been introduced during the 2·7 Ga collision of the western Slave Craton domain including the thick plume-derived deep lithospheric mantle layer and the eastern domain with its highly depleted lithosphere. This would also be consistent with the observation that volatile-rich eclogites occur at shallow depths in the mantle (T_{Krogh} = 685–855°C, corresponding to depths of ~85–115 km along a 40 mW/m^2 geotherm), where the bulk of dehydration and production of solute-rich melts in a subducting slab might be expected to occur (Becker *et al.*, 2000; Hermann *et al.*, 2006). Their negative Eu anomalies might indicate that the fluid was derived from the shallow portion of the slab that experienced plagioclase fractionation. The presence of carbonate in VR67112b requires a carbonated source.

High $^{87}Sr/^{86}Sr$ in cpx in YK1911 is probably the consequence of isotopic equilibration with high-Rb/Sr phlogopite after long-term radiogenic ingrowth, while Hf addition led to retarded ingrowth of radiogenic Hf.

These systematics, combined with radiogenic Nd appear inconsistent with the involvement of sediments in the petrogenesis of this sample (e.g. Perfit *et al.*, 1980; Vervoort *et al.*, 1999) or a hydrous fluid such as those responsible for MARID metasomatism in the Kaapvaal craton (Konzett *et al.*, 1998). Whatever the origin of the fluids, the apparent Hf mobility suggests that they were not in equilibrium with a rutile-bearing source and also that they were solute-rich in nature (i.e. hydrous melts, able to dissolve HFSE), and the relatively high HREE abundances of the volatile-rich eclogites indicate a garnet-free source, such as amphibolite. This allowed evolution of the sample at relatively high time-integrated Sm/Nd.

SUMMARY AND CONCLUSIONS

(1) The Lac de Gras kimberlites carried abundant eclogite and pyroxenite xenoliths to the surface. Three main eclogite types are distinguished in terms of major-element composition and trace element

patterns: high-Mg, high-Ca, and low-Mg eclogites. The garnets of all eclogite types have anti-correlated Mg-number and Yb, pointing to olivine fractionation as a controlling factor in the formation of their precursor rocks. Their flat or positively sloped HREE patterns qualitatively indicate that the melt parental to the precursor rocks was not in equilibrium with a garnet-bearing residue.

(2) Reconstructed high-Mg eclogites and high-Ca eclogites have flat HREE patterns, positive Pb and Sr anomalies and low Zr/Sm similar to oceanic gabbros reported in the literature. High-Mg eclogites have variably low HREE contents and some have small positive Eu anomalies, possibly suggestive of more primitive, relatively plagioclase-rich protoliths, whereas high-Ca eclogites have higher HREE abundances and small or absent Eu anomalies that require more cpx- and/or melt-rich protoliths, if a subduction origin is assumed.

(3) Low-Mg eclogites have distinctive trace-element patterns that show a marked positive slope in the HREE and subchondritic Zr/Hf. They resemble some Archaean second-stage melts ('boninites') and their protoliths appear to have formed from a previously depleted source.

(4) After formation, the eclogites were subject to a variety of processes. Most have low ratios of fluid-mobile vs less fluid-mobile elements, possibly as a result of dehydration of the protoliths. In addition, some of the low-Mg and high-Ca eclogites have low LREE/HREE consistent with partial melt loss. Whereas the low-Mg eclogites show concomitant enrichment in La, Nb and Zr, some high-Mg and high-Ca eclogites show evidence for variable and unsystematic (decoupled) LREE and Nb addition.

(5) Isotopically, the trace-element characteristics of the different eclogite types translate into lower ε_{Nd} for high-Mg eclogites (negative slope in MREE = lower Sm/Nd) than for low-Mg eclogites (positive slope in MREE = higher Sm/Nd). Within the low-Mg group, samples that show evidence for metasomatism (low Lu/Hf and Sm/Nd) have lower ε_{Nd} and ε_{Hf} than a sample that was apparently not metasomatized. Both Nd and Hf addition can be dated to ~1·7 Ga if identical initial isotope compsitions are assumed for the low-Mg eclogites. In contrast, the relatively constant and depleted mantle-like $^{87}Sr/^{86}Sr$ of eclogitic cpx, despite variable Nd and Hf isotope compositions and parent–daughter ratios, suggests recent input of juvenile material.

(6) Garnet and cpx in pyroxenites show major-element relationships different from those in eclogites. Therefore, these two rock types are probably not related by fractionation processes. The presence of opx precludes direct crystallization from slab-derived melts. Pyroxenites may be the product of (?slab-derived) melts hybridized during assimilation of peridotitic mantle.

(7) Garnets in phlogopite- and carbonate-bearing eclogites have extreme isotopic compositions, including the most radiogenic Nd and Hf in the dataset. Negative Eu anomalies may point to the involvement of a crustal protolith. Highly radiogenic Sr, radiogenic Nd and unradiogenic Hf in the reconstructed phlogopite-bearing sample combined with high HREE abundances and evidence for Hf mobility may indicate involvement of solute-rich fluids originating in a garnet- and rutile-free source.

ACKNOWLEDGEMENTS

Help in the clean laboratories and with the analytical facilities by S. Elhlou, C. Lawson, A. Sharma, P. Wieland and M. Zhang is greatly appreciated. Bill Griffin is thanked for his support and for agreeing to review several versions of the manuscript, despite disagreeing with many of the conclusions presented here. The paper benefited greatly from the detailed and constructive reviews provided by the editors, Gareth Davies and Marjorie Wilson, and by Matthias Barth, Larry Heaman and an anonymous reviewer. This work was funded by a Macquarie University International Postgraduate Award and Postgraduate Research Fund (S.A.), by an ARC SPIRT grant sponsored by Kennecott Canada Inc., and by ARC Large and Discovery Grants to S.Y.O'R. Analytical data were obtained using instrumentation funded by ARC LIEF, and DEST Systemic Infrastructure Grants, industry partners and Macquarie University. This is Publication 481 from the ARC National Key Centre for Geochemical Evolution and Metallogeny of Continents (www.es.mq.edu.au/GEMOC/).

SUPPLEMENTARY DATA

Supplementary data for this paper are available at *Journal of Petrology* online.

REFERENCES

Adam, J., Green, T. H., Sie, S. H. & Ryan, C. G. (1997). Trace element partitioning between aqueous fluids, silicate melts and minerals. *European Journal of Mineralogy* **9**, 569–584.

Aulbach, S., Stachel, T., Viljoen, K. S., Brey, G. P. & Harris, J. W. (2002). Eclogitic and websteritic diamond sources beneath the Limpopo Belt—is slab-melting the link? *Contributions to Mineralogy and Petrology* **143**, 56–70.

Aulbach, S., Griffin, W. L., Pearson, N. J., O'Reilly, S. Y., Kivi, K. & Doyle, B. (2003). Origins of eclogites beneath the central Slave Craton. Extended Abstract. 8th International Kimberlite Conference, Victoria, BC. Abstract no. FLA-0011.

Aulbach, S., Griffin, W. L., Pearson, N. J., O'Reilly, S. Y. & Kivi, K. (2004*a*). Mantle formation and evolution, Slave Craton: constraints

from HSE abundances and Re–Os isotope systematics of sulfide inclusions in mantle xenocrysts. *Chemical Geology* **208**, 61–88.

Aulbach, S., Griffin, W. L., O'Reilly, S. Y. & McCandless, T. E. (2004*b*). Genesis and evolution of the lithospheric mantle beneath the Buffalo Head Terrane, Alberta (Canada). *Lithos* **77**, 413–451.

Aulbach, S., Griffin, W. L., Pearson, N. J., O'Reilly, S. Y. & Doyle, B. (2007). Lithosphere formation in the central Slave Craton (Canada): plume subcretion or lithosphere accretion? *Contributions to Mineralogy and Petrology*, (in press). doi: 10.1007/s00410-007-0200-1.

Barth, M. G., Rudnick, R. L., Horn, I., McDonough, W. F., Spicuzza, M. J., Valley, J. W. & Haggerty, S. E. (2001). Geochemistry of xenolithic eclogites from West Africa, Part I: A link between low MgO eclogites and Archean crust formation. *Geochimica et Cosmochimica Acta* **65**, 1499–1527.

Barth, M. G., Foley, S. F. & Horn, I. (2002*a*). Partial melting in Archean subduction zones: constraints from experimentally determined trace element partition coefficients between eclogitic minerals and tonalitic melts under upper mantle conditions. *Precambrian Research* **113**, 323–340.

Barth, M. G., Rudnick, R. L., Horn, I., McDonough, W. F., Spicuzza, M. J., Valley, J. W. & Haggerty, S. E. (2002*b*). Geochemistry of xenolithic eclogites from West Africa, part 2: Origins of the high MgO eclogites. *Geochimica et Cosmochimica Acta* **66**, 4325–4345.

Beard, B. L., Fraracci, K. N., Taylor, L. A., Snyder, G. A., Clayton, R. A., Mayeda, T. K. & Sobolev, N.V. (1996). Petrography and geochemistry of eclogites from the Mir kimberlite, Yakutia, Russia. *Contributions to Mineralogy and Petrology* **125**, 293–310.

Becker, H. (1996). Geochemistry of garnet peridotite massifs from lower Austria and the composition of deep lithosphere beneath a Palaeozoic convergent plate margin. *Chemical Geology* **134**, 49–65.

Becker, H., Jochum, K. P. & Carlson, R. W. (2000). Trace element fractionation during dehydration of eclogites from high-pressure terranes and the implications for element fluxes in subduction zones. *Chemical Geology* **163**, 65–99.

Bell, K. & Tilton, G. R. (2002). Probing the mantle: The story from carbonatites. *EOS Transactions, American Geophysical Union* **83**, 275–277.

Benoit, M., Polvé, M. & Ceuleneer, G. (1996). Trace element and isotopic characterisation of mafic cumulates in a fossil mantle diapir (Oman ophiolite). *Chemical Geology* **134**, 199–214.

Bleeker, W. (2003). The late Archean record: a puzzle in ca. 35 pieces. *Lithos* **71**, 99–134.

Bleeker, W., Ketchum, J. W. F., Jackson, V. A. & Villeneuve, M. (1999). The central Slave Basement Complex. Part I: Its structural topology and autochthonous core. *Canadian Journal of Earth Sciences* **36**, 1083–1109.

Blichert-Toft, J. & Albarède, F. (1997). The Lu–Hf isotope geochemistry of chondrites and the evolution of the mantle–crust system. *Earth and Planetary Science Letters* **148**, 243–258.

Blichert-Toft, J., Chauvel, C. & Albarède, F. (1997). Separation of Hf and Lu for high precision isotope analysis of rock samples by magnetic sector-multiple collector ICP-MS. *Contributions to Mineralogy and Petrology* **127**, 248–260.

Brey, G. P. & Köhler, T. (1990). Geothermobarometry in four-phase lherzolites II. New thermobarometers, and practical assessment of existing thermobarometers. *Journal of Petrology* **31**, 1353–1378.

Brey, G. P., Köhler, T. & Nickel, K. G. (1990). Geothermobarometry in four-phase lherzolites I. Experimental results from 10 to 60 kb. *Journal of Petrology* **31**, 1313–1352.

Caporuscio, F. & Smyth, J. (1990). Trace element crystal chemistry of mantle eclogites. *Contributions to Mineralogy and Petrology* **105**, 550–561.

Carbno, G. B. & Canil, D. (2002). Mantle structure beneath the SW Slave Craton, Canada: constraints from garnet geochemistry in the Drybones Bay Kimberlite. *Journal of Petrology* **43**, 129–142.

Coleman, R. G., Lee, E. D., Beatty, L. B. & Brannock, W. W. (1965). Eclogites and eclogites: their differences and similarities. *Geological Society of America Bulletin* **76**, 483–508.

Creaser, R. A., Grütter, H., Carlson, J. & Crawford, B. (2004). Macrocrystal phlogopite Rb–Sr dates for the Ekati property kimberlites, Slave Province, Canada: evidence for multiple intrusive episodes in the Paleocene and Eocene. *Lithos* **76**, 399–414.

Davies, R. M., Griffin, W. L., Pearson, N. J., Andrew, A. S., Doyle, B. J. & O'Reilly, S. Y. (1999). Diamonds from the deep: Pipe DO-27, Slave Craton, Canada. In: Gurney, J. J., Gurney, J. L., Pascoe, M. D. & Richardson, S. H. (eds) *Proceedings of the 7th International Kimberlite Conference*. Cape Town: Red Roof Design, pp. 148–155.

Davies, R. M., Griffin, W. L., O'Reilly, S. Y. & Doyle, B. J. (2004). Mineral inclusions and geochemical characteristics of microdiamonds from the DO27, A154, A21, A418, DO18, DD17 and Ranch Lake kimberlites at Lac de Gras, Slave Craton, Canada. *Lithos* **77**, 39–55.

Davis, W. J. & Hegner, E. (1992). Neodymium isotopic evidence for the tectonic assembly of Late Archean crust in the Slave Province, northwest Canada. *Contributions to Mineralogy and Petrology* **111**, 493–504.

Davis, W. J., Jones, A. G., Bleeker, W. & Grutter, H. (2003). Lithosphere development in the Slave craton: a linked crustal and mantle perspective. *Lithos* **71**, 575–589.

Dawson, J. B. (1984). Contrasting types of upper-mantle metasomatism. In: Kornprobst, J. (ed.), *Kimberlites II: The Mantle and Crust–Mantle Relationships*. Amsterdam: Elsevier, pp. 289–294.

DePaolo, D. J. (1981). Neodymium isotopes in the Colorado Front Range and crust–mantle evolution in the Proterozoic. *Nature* **291**, 193–196.

Erlank, A. J. & Kushiro, I. (1970). Potassium contents of synthetic pyroxenes at high temperatures and pressures. *Carnegie Institution of Washington Yearbook* **68**, 433–439.

Foley, S. F., Barth, M. G. & Jenner, G. A. (2000). Rutile/melt partition coefficients for trace elements and an assessment of the influence of rutile on the trace element characteristics of subduction zone magmas. *Geochimica et Cosmochimica Acta* **64**, 933–938.

Foley, S. F., Buhre, S. & Jacob, D. E. (2003). Evolution of the Archaean crust by delamination and shallow subduction. *Nature* **421**, 249–252.

Graham, I., Burgess, J. L., Bryan, D., Ravenscroft, P. J., Thomas, E., Doyle, B. J., Hopkins, R. & Armstrong, K. A. (1999). Exploration history and geology of the Diavik Kimberlites, Lac de Gras, Northwest Territories, Canada. In: Gurney, J. J., Gurney, J. L., Pascoe, M. D. & Richardson, S. H. (eds) *Proceedings of the 7th International Kimberlite Conference*. Cape Town: Red Roof Design, pp. 262–279.

Green, D. H. & Wallace, M. E. (1988). Mantle metasomatism by ephemeral carbonatite melts. *Nature* **336**, 459–462.

Green, T. H., Blundy, J. D., Adam, J. & Yaxley, G. M. (2000). SIMS determination of trace element partition coefficients between garnet, clinopyroxene and hydrous basaltic liquids at 2–7·5 GPa and 1080–1200°C. *Lithos* **53**, 165–187.

Griffin, W. L. & O'Reilly, S. Y. (2007). Cratonic lithospheric mantle: Is anything subducted? *Episodes* **30**(1), 43–53.

Griffin, W. L., Wass, S. Y. & Hollis, J. D. (1984). Ultramafic xenoliths from Bullenmerri and Gnotuk maars. Victoria, Australia: petrology of a sub-continental crust–mantle transition. *Journal of Petrology* **25**, 53–87.

Griffin, W. L., Doyle, B. J., Ryan, C. G., Pearson, N. J., O'Reilly, S. Y., Davies, R., Kivi, K., van Achterbergh, E. & Natapov, L.M. (1999).

Layered mantle lithosphere in the Lac de Gras Area, Slave Craton: composition, structure and origin. *Journal of Petrology* **40**, 705–727.

Griffin, W. L., Pearson, N. J., Belousova, E., Jackson, S. E., van Achterbergh, E., O'Reilly, S. Y. & Shee, S. R. (2000). The Hf isotope composition of cratonic mantle: LAM-MC-ICPMS analysis of zircon megacrysts in kimberlites. *Geochimica et Cosmochimica Acta* **64**, 133–147.

Griffin, W. L., O'Reilly, S. Y., Doyle, B. J., Pearson, N. J., Coopersmith, H., Kivi, K., Malkovets, V. & Pokhilenko, N. (2004). Lithosphere mapping beneath the North American plate. *Lithos* **77**, 873–922.

Grütter, H. S., Apter, D. B. & Kong, J. (1999). Crust–mantle coupling: evidence from mantle-derived xenocrystic garnets. In: Gurney, J. J., Gurney, J. L., Pascoe, M. D. & Richardson, S. H. (eds) *Proceedings of the 7th International Kimberlite Conference*. Cape Town: Red Roof Design, pp. 307–312.

Hart, S. R., Blusztajn, J., Dick, H. J. B., Meyer, P. S. & Muehlenbachs, K. (1999). The fingerprint of seawater circulation in a 500-meter section of ocean crust gabbros. *Geochimica et Cosmochimica Acta* **63**, 4059–4080.

Harte, B. & Kirkley, M. B. (1997). Partitioning of trace elements between clinopyroxene and garnet: Data from mantle eclogites. *Chemical Geology* **136**, 1–24.

Heaman, L. M., Creaser, R. A. & Cookenboo, H. O. (2002). Extreme enrichment of high field strength elements in Jericho eclogite xenoliths: A cryptic record of Paleoproterozoic subduction, partial melting, and metasomatism beneath the Slave craton, Canada. *Geology* **30**, 507–510.

Heaman, L. M., Kjarsgaard, B. A. & Creaser, R. A. (2004). The temporal evolution of North American kimberlites. *Lithos* **76**, 377–397.

Heaman, L. M., Creaser, R. A., Cookenboo, H. O. & Chacko, T. (2006). Multi-stage modification of the northern Slave mantle lithosphere: Evidence from zircon- and diamond-bearing eclogite xenoliths entrained in Jericho Kimberlite. *Journal of Petrology* **47**, 821–858.

Hermann, J., Cpandler, C., Hack, A. & Korsakov, A. (2006). Aqueous fluids and hydrous melts in high-pressure and ultra-high pressure rocks: implications for element transfer in subduction zones. *Lithos* **92**, 399–417.

Hills, D. V. & Haggerty, S. E. (1989). Petrochemistry of eclogites from the Koidu Kimberlite Complex, Sierra Leone. *Contributions to Mineralogy and Petrology* **103**, 397–422.

Hoffman, P. F. (1989). Precambrian geology and tectonic history of North America. In: Bally, A. & Palmer, A. (eds) *The Geology of North America—An Overview*. Boulder, CO: Geological Society of America, pp. 447–512.

Ireland, T. R., Rudnick, R. L. & Spetsius, Z. (1994). Trace-elements in diamond inclusions from eclogites reveal link to Archean granites. *Earth and Planetary Science Letters* **128**, 199–213.

Irvine, G. J., Pearson, D. G., Kjarsgaard, B. A., Carlson, R. W., Kopylova, M. G. & Dreibus, G. (2003). Evolution of the lithospheric mantle beneath Northern Canada: a Re–Os isotope and PGE study of kimberlite-derived peridotite xenoliths from Somerset Island and a comparison to the Slave and Kaapvaal cratons. *Lithos* **71**, 461–488.

Isachsen, C. E. & Bowring, S. A. (1994). Evolution of the Slave craton. *Geology* **22**, 917–920.

Jacob, D. E. (2004). Nature and origin of eclogite xenoliths from kimberlites. *Lithos* **77**, 295–316.

Jacob, D. E. & Foley, S. F. (1999). Evidence for Archean ocean crust with low high field strength element signature from diamondiferous eclogite xenoliths. *Lithos* **48**, 317–336.

Jacob, D., Jagoutz, E., Lowry, D., Mattey, D. & Kudrjavtseva, G. (1994). Diamondiferous eclogites from Siberia—remnants of Archean oceanic-crust. *Geochimica et Cosmochimica Acta* **58**, 5191–5207.

Jacob, D. E., Fung, A., Jagoutz, E. & Pearson, D. G. (2003). Petrology and geochemistry of eclogite xenoliths from the Ekati kimberlites area. Extended Abstract. 8th International Kimberlite Conference, Victoria, BC. Abstract no. FLA.239.

Jacob, D. E., Bizimis, M. & Salters, V. J. M. (2005). Lu–Hf and geochemical systematics of recycled ancient oceanic crust: evidence from Roberts Victor eclogites. *Contributions to Mineralogy and Petrology* **148**, 707–720.

Jerde, E. A., Taylor, L. A., Crozaz, G., Sobolev, N. V. & Sobolev, V. N. (1993). Diamondiferous eclogites from Yakutia, Siberia—evidence for a diversity of protoliths. *Contributions to Mineralogy and Petrology* **114**, 189–202.

Jones, A. G., Ferguson, I. J., Chave, A. D., Evans, R. L. & McNeice, G. W. (2001). The electric lithosphere of the Slave craton. *Geology* **29**, 423–426.

Kelemen, P. B., Shimizu, N. & Dunn, T. (1993). Relative depletion of niobium in some arc magmas and the continental-crust-partitioning of K, Nb, La and Ce during melt/rock reaction in the upper-mantle. *Earth and Planetary Science Letters* **120**, 111–134.

Kinzler, R. J. (1997). Melting of mantle peridotite at pressures approaching the spinel to garnet transition: Application to mid-ocean ridge basalt petrogenesis. *Journal of Geophysical Research* **102**, 853–874.

Klemme, S., van der Laan, S. R., Foley, S. F. & Guenther, D. (1995). Experimentally determined trace and minor element partitioning between clinopyroxene and carbonatite melt under upper mantle conditions. *Earth and Planetary Science Letters* **133**, 439–448.

Konzett, J., Armstrong, R. A., Sweeney, R. J. & Compston, W. (1998). The timing of MARID metasomatism in the Kaapvaal mantle; an ion probe study of zircons from MARID xenoliths. *Earth and Planetary Science Letters* **160**, 133–145.

Kopylova, M. G., Russell, J. K. & Cookenboo, H. (1999). Mapping the lithopshere beneath the north central Slave Craton. In: Gurney, J. J., Gurney, J. L., Pascoe, M. D. & Richardson, S. H. (eds) *Proceedings of the 7th International Kimberlite Conference*. Cape Town: Red Roof Design, pp. 468–479.

Krogh, E. (1988). The garnet–clinopyroxene iron–magnesium geothermometer—a reinterpretation of existing experimental data. *Contributions to Mineralogy and Petrology* **99**, 44–48.

Kusky, T. M. (1989). Accretion of Archean Slave Province. *Geology* **17**, 63–67.

LeCheminant, A. N. & Heaman, L. M. (1989). Mackenzie igneous events, Canada: Middle Proterozoic hotspot magmatism associated with ocean opening. *Earth and Planetary Science Letters* **96**, 38–48.

LeCheminant, A. N., Richardson, D. G., DiLabio, R. N. W. & Richardson, K. A. (1996). La recherche de diamants au Canada. *Geological Survey of Canada, Open File* **3228**, 268pp.

MacGregor, I. D. & Carter, J. L. (1970). The chemistry of clinopyroxenes and garnets of eclogite and peridotite xenoliths from the Roberts Victor mine, South Africa. *Physics of the Earth and Planetary Interiors* **3**, 391–397.

MacGregor, I. D. & Manton, W. I. (1986). Roberts Victor eclogites: ancient oceanic crust. *Journal of Geophysical Research* **91**, 14063–14079.

MacKenzie, J. M. & Canil, D. (1999). Composition and thermal evolution of cratonic mantle beneath the central Archean Slave Province, NWT, Canada. *Contributions to Mineralogy and Petrology* **134**, 313–324.

McCandless, T. E. & Gurney, J. J. (1989). Sodium in garnet and potassum in clinopyroxene: criteria for classifying mantle eclogites. In: Ross, J. (ed.), *Kimberlites and Related Rocks*. Carlton: Blackwell, pp. 827–832.

McDonough, W. F. & Sun, S.-S. (1995). The composition of the Earth. *Chemical Geology* **120**, 223–253.

Navon, O. & Stolper, E. (1987). Geochemical consequences of melt percolation: the upper mantle as a chromatographic column. *Journal of Geology* **95**, 285–307.

Nikogosian, I. K. & Sobolev, A. V. (1997). Ion-microprobe analysis of melt inclusions in olivine: experience in estimating the olivine–melt partition coefficients of trace elements. *Geochemistry International* **35**, 119–126.

Norman, M. D., Griffin, W. L., Pearson, N. J., Garcia, M. O. & O'Reilly, S. Y. (1998). Quantitative analysis of trace element abundances in glasses and minerals: a comparison of laser ablation inductively coupled plasma mass spectrometry, solution inductively coupled plasma mass spectrometry, proton microprobe and electron microprobe data. *Journal of Analytical Atomic Spectrometry* **13**, 477–482.

Norman, M. D., Garcia, M. O. & Pietruszka, A. J. (2005). Trace-element distribution coefficients for pyroxenes, plagioclase, and olivine in evolved tholeiites from the 1955 eruption of Kilauea Volcano, Hawai'i, and petrogenesis of differentiated rift-zone lavas. *American Mineralogist* **90**, 888–899.

O'Hara, M. J. & Herzberg, C. (2002). Interpretation of trace element and isotope features of basalts: Relevance of field relations, petrology, major element data, phase equilibria, and magma chamber modeling in basalt petrogenesis. *Geochimica et Cosmochimica Acta* **66**, 2167–2191.

Padgham, W. A. & Fyson, W. K. (1992). The Slave Province: a distinct craton. *Canadian Journal of Earth Sciences* **29**, 2072–2086.

Pearson, D. G., Davies, G. R. & Nixon, P. H. (1993). Geochemical constraints on the petrogenesis of diamond facies pyroxenites from the Beni Bousera peridotite massif, North Morocco. *Journal of Petrology* **34**, 125–172.

Pearson, N. J., Griffin, W. L., Doyle, B. J., O'Reilly, S. Y., van Achterbergh, E. & Kivi, K. (1999). Xenoliths from kimberlite pipes of the Lac de gras area, Slave Craton, Canada. In: Gurney, J. J., Gurney, J. L., Pascoe, M. D. & Richardson, S. H. (eds) Proceedings of the 7th International Kimberlite Conference. Cape Town: Red Roof Design, pp. 644–658..

Perfit, N. R., Gust, D. A., Bence, A. E., Arculus, R. J. & Taylor, S. R. (1980). Chemical characteristics of island-arc basalts: implications for mantle sources. *Chemical Geology* **30**, 227–256.

Polat, A., Hofmann, A. W. & Rosing, M. T. (2002). Boninite-like volcanic rocks in the 3·7–3·8 Ga Isua greenstone belt, West Greenland: geochemical evidence for intra-oceanic subduction zone processes in the early Earth. *Chemical Geology* **184**, 231–254.

Poudjom Djomani, Y. H., Griffin, W. L., O'Reilly, S. Y. & Doyle, B. J. (2005). Lithospheric domains and controls on kimberlite emplacement, Slave Province, Canada; evidence from elastic thickness and upper mantle composition. *Geochemistry, Geophysics, Geosystems* **6**, doi:10.1029/2005GC0009978.

Presnall, D. C., Gudfinnsson, G. H. & Walter, M. J. (2002). Generation of mid-ocean ridge basalts at pressures from 1 to 7 GPa. *Geochimica et Cosmochimica Acta* **66**, 2073–2090.

Schmidberger, S. S., Heaman, L. M., Simonetti, A., Creaser, R. A. & Cookenboo, H. O. (2005). Formation of Paleoproterozoic eclogitic mantle, Slave Province (Canada): Insights from in-situ Hf and U–Pb isotopic analyses of mantle zircons. *Earth and Planetary Science Letters* **240**, 621–633.

Schmidberger, S. S., Simonetti, A., Heaman, L. M., Creaser, R. A. & Whiteford, S. (2007). Lu–Hf, in-situ Sr and Pb isotope and trace element systematics for mantle eclogites from the Diavik diamond mine: Evidence for Paleoproterozoic subduction beneath the Slave craton, Canada. *Earth and Planetary Science Letters* **254**, 55–68.

Schulze, D. J. & Helmstaedt, H., (1988). Coesite-sanidine eclogites from kimberlite: products of mantle fractionation or subduction? *Journal of Geology*, **96**, 435–443.

Smithies, R. H., Champion, D. C. & Sun, S. S. (2004). The case for Archaean boninites. *Contributions to Mineralogy and Petrology* **147**, 705–721.

Smyth, J. R., Caporuscio, F. A. & McCormick, T. C. (1989). Mantle eclogites: evidence of igneous fractionation in the mantle. *Earth and Planetary Science Letters* **93**, 133–141.

Sobolev, N. V. & Lavrent'yev, Y. G. (1971). Isomorphic sodium admixture in garnets formed at high pressure. *Contributions to Mineralogy and Petrology* **31**, 1–12.

Stalder, R., Foley, S. F., Brey, G. P. & Horn, I. (1998). Mineral aqueous fluid partitioning of trace elements at 900–1200°C and 3·0–5·7 GPa: New experimental data for garnet, clinopyroxene, and rutile, and implications for mantle metasomatism. *Geochimica et Cosmochimica Acta* **62**, 1781–1801.

Sun, S.-S. & McDonough, W. F. (1989). Chemical and isotopic systematics of oceanic basalts: implications for mantle compositions and processes. In: Saunders, A. D. & Norris, M. J. (eds) *Magmatism in the Ocean Basins. Geological Society, London, Special Publications* **42**, 313–345.

Taura, H., Yurimoto, H., Kurita, K. & Sueno, S. (1998). Pressure dependence on partition coefficients for trace elements between olivine and the coexisting melts. *Physics and Chemistry of Minerals* **25**, 469–484.

Taylor, L. A. & Neal, C. R. (1989). Eclogites with oceanic crustal and mantle signatures from the Bellsbank kimberlite, South Africa, Part I: Mineralogy, petrography, and whole rock chemistry. *Journal of Geology* **97**, 551–567.

van Achterbergh, E., Ryan, C. G. & Griffin, W. L. (1999). Glitter: on line intensity reduction for the laser ablation inductively coupled plasma spectrometry. Abstract. 9th V. M. Goldschmidt Conference, LPI, Boston, MA, 905 pp. Abstract no. 7215.

van Breemen, O., Davis, W. J. & King, J. E. (1992). Temporal distribution of granitoid plutonic rocks in the Archean Slave Province, Northwest Canadian Shield. *Canadian Journal of Earth Sciences* **29**, 2186–2199.

Vervoort, J. D., Patchett, P. J., Blichert-Toft, J. & Albarède, F. (1999). Relationship between Lu–Hf and Sm–Nd isotopic systems in the global sedimentary system. *Earth and Planetary Science Letters* **168**, 79–99.

Viljoen, K. S., Smith, C. B. & Sharp, Z. D. (1996). Stable and radiogenic isotope study of eclogite xenoliths from the Orapa kimberlite, Botswana. *Chemical Geology* **131**, 235–255.

Walter, M. J. (1998). Melting of garnet peridotite and the origin of komatiite and depleted lithosphere. *Journal of Petrology* **39**, 29–60.

Wasserburg, G. J., Jacobsen, S. B., DePaolo, D. J., McCulloch, M. T. & Wen, T. (1981). Precise determination of Sm/Nd ratios, Sm and Nd isotopic abundances in standard solutions. *Geochimica et Cosmochimica Acta* **45**, 2311–2323.

Westerlund, K. J., Shirey, S. B., Richardson, S. H., Carlson, R. W., Gurney, J. J. & Harris, J. W. (2006). A subduction wedge origin for Paleoarchean peridotitic diamonds and harzburgites from the Panda kimberlite, Slave craton, evidence from Re–Os isotope systematics. *Contributions to Mineralogy and Petrology* **152**, 275–294.